# Radiative $^3$He capture in $^{12}$C and $^{16}$O†

H. D. Shay,* R. E. Peschel, J. M. Long, and D. A. Bromley
*Wright Nuclear Structure Laboratory, Yale University, New Haven, Connecticut 06520*
(Received 8 September 1972)

A comprehensive study has been completed on the $^3$He radiative-capture reactions $^9$Be($^3$He,$\gamma$)$^{12}$C, leading to the first four states of $^{12}$C, and $^{13}$C($^3$He,$\gamma$)$^{16}$O, leading to the first five states in $^{16}$O. Excitation functions have been extended to excitations of 45 and 35 MeV, respectively, by bombarding natural $^9$Be and isotopically enriched $^{13}$C targets with $^3$He from the Wright Nuclear Structure Laboratory MP tandem accelerator. Angular distributions have been taken at many key energies. These experiments utilized a large NaI(Tl) $\gamma$-radiation detector and plastic-scintillator cosmic-ray anticoincidence shield built as part of this program, and the IBM 360/44 on-line data acquisition system. Several resonances have been found. The experiment appears to confirm the role of 3p-3h configurations immediately above the giant resonances of $^{12}$C and $^{16}$O. Microscopic $R$-matrix calculations based on the Wang and Shakin 1p-1h and 3p-3h $^{16}$O wave functions have been conducted. Detailed comparison of these calculations with our data and $^{15}$N($p,\gamma_0$)$^{16}$O data suggests that the source of much of the intermediate structure seen in the $^{16}$O giant resonance may stem from the mixing of 1p-1h doorway configurations with 3p-3h configurations.

[NUCLEAR REACTIONS $^9$Be($^3$He,$\gamma$), $E$=3–26 MeV; $^{13}$C($^3$He,$\gamma$), $E$=3–16 MeV; measured $\sigma(E;E_\gamma,\theta)$. $^{13}$C, $^{16}$O deduced levels $J$, $\pi$, resonance parameters. Natural $^9$Be target. Enriched $^{13}$C target.]

## 1. INTRODUCTION

Microscopic models of giant-dipole-resonance states have enjoyed moderate success in light nuclei. Several calculations[1–3] have demonstrated that, when the residual particle-hole interaction is considered, the 1p-1h model predicts correctly the excitation-energy centroid of the giant dipole resonances and the enhancement of the electric dipole $\gamma$-absorption cross sections of doubly magic nuclei $^{12}$C, $^{16}$O, and $^{40}$Ca. Detailed calculations[4–6] of their photonuclear cross sections and of the angular distributions (or polarizations) of the nucleon emitted following photoabsorption have been conducted within the framework of this 1p-1h model. These calculations characteristically reproduce the general envelope of the observed photonuclear cross sections and the shape of the product-nucleon angular distributions, which are dominated mainly by the electric dipole terms. This degree of success primarily reflects the fact that the electromagnetic interaction is characterized by a one-body operator and that these light nuclei are, to first approximation, reasonably described by doubly-closed-shell cores. The 1p-1h $J^\pi=1^-$, $T=1$ states carrying enhanced dipole strength may, thus, be viewed as doorway states for photodisintegration (or, alternatively, radiative capture). The radiative-capture[6–11] and photodisintegration[12,13] experiments in $^{12}$C and in $^{16}$O reveal intermediate structure which is not predicted by these detailed 1p-1h calculations. Significantly, the structure observed in the total cross sections of these reactions is not accompanied by variations of the shape of the angular distributions measured at energies corresponding to specific structural features in the excitation curves. The predicted integrated $(\gamma,p)$ or $(\gamma,n)$ cross sections exceed the observed value typically by a factor of 2.

Gillet, Melkanoff, and Raynal[14] have suggested that much of the structure in the giant resonance of $^{16}$O may arise from $n$p-$n$h states and, specifically, that 2p-2h admixtures split the 22-MeV peak. Recently Wang and Shakin[15] proposed that the intermediate structure of the $^{16}$O giant resonance arises primarily from 3p-3h secondary doorway states. In their model the giant-resonance 1p-1h doorway states are strongly mixed by residual interactions only with the 3p-3h configurations of the same region of excitation. Inasmuch as these 3p-3h configurations are the only compound-nuclear states assumed to be mixing with the 1p-1h giant-resonance doorway states, they are designated secondary doorway states. At the closure of the 1p shell, 3p-3h configurations (with particles in the $2s$-$1d$ shell) are the lowest-order $n$p-$n$h configurations which may couple to form $1^-$ states without the promotion of a particle across a major shell. With this secondary door-

way hypothesis and assumptions regarding the structure of the 3p-3h states in this region, Wang and Shakin have successfully reproduced the intermediate structure and normalization in the $^{16}$O photonuclear disintegration experiment.

The descriptions of the $^{12}$C and $^{16}$O ground states as doubly-closed $1p_{3/2}$ and $1p_{1/2}$ cores represent, at best, somewhat tenuous approximations, and the description of the $^9$Be and $^{13}$C ground states as 3h states represents an even poorer approximation. To the extent that these descriptions have validity, however, helion ($^3$He) capture experiments on $^9$Be and $^{12}$C can explore directly the mixing of 1p-1h and 3p-3h configurations in and above the giant-resonance regions of $^{12}$C and $^{16}$O, respectively. Helion capture can, then, provide an independent test of the secondary doorway hypothesis and, particularly, of Wang and Shakin's $^{16}$O 1p-1h and 3p-3h wave functions. Helion capture is the preferable experimental approach to these studies; triton-capture experiments are not feasible since $^{13}$N and $^9$B are not stable nuclei. The inverse experiments [$(\gamma, ^3\text{He})$ and $(\gamma, t)$] are less promising since the necessity of thin targets, the corresponding small cross sections, and the low duty cycle of presently available electron accelerators, would result in unacceptibly low experimental counting rates.

In this paper we report the results of recent helion-capture studies $^9$Be $(^3\text{He}, \gamma)^{12}$C and $^{13}$C-$(^3\text{He}, \gamma)^{16}$O performed at this laboratory. The MP tandem Van de Graaff accelerator used provided a helion beam with energies continuously variable from below 3 MeV to above 30 MeV and with resolution typically of one part in $10^4$. An exploratory study of $^{10}\text{B}(d, \gamma)^{12}$C was also conducted. As part of a continuing program of radiative-capture experiments we have constructed a specially designed beam line and a large NaI(Tl) detector assembly and have developed electronic and on-line data acquisition hardware and software. Our data suggest that 3p-3h configurations do play a significant role in the giant resonances of $^{12}$C and $^{16}$O. Resonances have been found which indicate long-lived states at excitations in the energy ranges 28 to 35 MeV and 25 to 29 MeV in the compound systems of $^{12}$C and $^{16}$O. Angular distributions of the radiative-capture $\gamma$ radiation taken over a wide range of energies delimit their spins and parities. We have completed an $R$-matrix calculation based on the 1p-1h, 3p-3h wave functions of Wang and Shakin which reproduced both the $^{15}\text{N}(p, \gamma_0)^{16}$O data of O'Connell[11] and our $^{13}\text{C}(^3\text{He}, \gamma_0)^{16}$O data. Our studies, thus, tend to support the application of the secondary doorway hypothesis to the upper half of the giant-resonance region in $^{16}$O.

## 2. EXPERIMENTAL TECHNIQUE

The experimental studies involved the detection of $\gamma$ radiation emitted from $^{12}$C or $^{16}$O nuclei formed following the capture of helions by $^9$Be or $^{13}$C nuclei, respectively. Because the solid angle subtended by the detector collimator was well defined, because the numbers of incident helions and target nuclei were accurately determined, and because the detector efficiency was essentially 100%, the total number of $\gamma$ photons detected constituted an absolute measurement of differential cross sections at a particular beam energy and detector angle. The choice of data reduction procedure constitutes the major uncertainty in assigning the over-all normalization of these data.

The detector [an anticoincidence shielded 29.2-cm-diam by 30.5-cm-deep NaI(Tl) spectrometer] and its defining collimator (with an angular acceptance of $\Delta\theta \leq 9°$) could be rotated about the target in a plane containing the beam axis to measure differential cross sections through the range of laboratory angles, 30 to 150°. Excitation functions have been measured at 90° for $3 \leq 26$ MeV and $3 \leq E_h \leq 16$ MeV for $^{12}$C and $^{16}$O, respectively. Angular distributions of the capture $\gamma$ radiation have been measured at many energies throughout these ranges. Since $\gamma$ deexcitation transitions to several low-lying states in $^{12}$C or $^{16}$O were resolved by the NaI(Tl) detector, the differential cross sections of several radiative-capture reaction channels were determined simultaneously.

Radiative-capture experiments, although straightforward in concept, are difficult in execution. Neutrons and lower-energy cascade $\gamma$ radiation from other nuclear reactions, either in the target or in parts of the beam line struck by the beam, can overwhelm the $\gamma$ detector with an enormous background rate. When conventional nuclear electronics are used in radiative capture experiments, the resulting pileup problem is often so severe that it is necessary to use a very low beam current and, consequently, the data acquisition rates may be extremely low.[7,16]. The use of slow pileup rejection circuitry results in the spurious rejection of a large fraction of valid events at a high count rate. The detection of cosmic rays poses an ever present background which frequently renders such a pileup rejection solution impractical. In the past, one method of sorting radiative-capture events from cosmic-ray events has been to surround the $\gamma$ detector [NaI(Tl)] with a thick plastic scintillator which would register the passage of cosmic-ray muons into the crystal. Events coincident in both the $\gamma$ detector and the plastic scintillator were then

rejected, but, unfortunately, a good fraction of the events of interest were also rejected by this technique. In such plastic scintillators the rate due to background neutrons has characteristically been $10^6$/sec under conditions in which the total rate in the crystal has been $10^5$/sec. Diener *et al.*[16] report that, because of random coincidences, the percentage of valid events rejected by the cosmic-ray veto rose from 38 to 52% as the crystal counting rate was changed from $1.2 \times 10^5$ to $4.6 \times 10^6$/sec. Such thick plastic scintillators do have the advantage of improving resolution by rejecting a substantial fraction of those events in which not all of the photon energy is deposited in the NaI(Tl) crystal, but, rather, some escapes into the plastic scintillator.[16] Several approaches have been used to discriminate against the cosmic-ray events without rejecting valid events. Suffert[17] placed lead shielding between the NaI(Tl) crystal and the plastic scintillator. Del Bianco and Lemaire[18] report the rejection of cosmic-ray events by a Cerenkov anticoincidence shield which is relatively insensitive to the neutron background. We describe below our resolution to these experimental difficulties.

The doubly charged helion beam was focused on thin self-supporting $^9$Be or $^{13}$C foils. During the acquisition of data, the beam struck nothing in the target room other than the target or the end of the heavily shielded Faraday cup. Thus, a neutron background could be generated only by nuclear reactions in the target itself. The total number of helions incident upon the target was determined by integrating the charge collected in an insulated and suppressed Faraday cup. The beam-current integration accuracy and linearity was checked with a precision current source and found to be better than 2–3%.

Target films of 50–100 $\mu$g/cm$^2$ were prepared by vacuum evaporation of pure $^9$Be or isotopically enriched $^{13}$C onto substrates coated with a thin layer of evaporated sodium chloride. These layers were floated off of the substrate in water and mounted on target frames. Successive layers were picked up on each target frame so that the resulting targets had thicknesses as great as 300 $\mu$g/cm$^2$. The thicknesses of these targets were determined by standard $\alpha$-gauge techniques. Such measurements of areal densities have an accuracy of better than 10%.[19] Several such target frames were finally stacked together within the target chamber so that effective targets as thick as 1.2 mg/cm$^2$ were available when required.

Figure 1 illustrates the spectrometer system. The front lead shield, 12.7 cm thick, was fitted with interchangeable, tapered lead collimators.

SCHEMATIC ILLUSTRATION OF EXPERIMENTAL APPARATUS

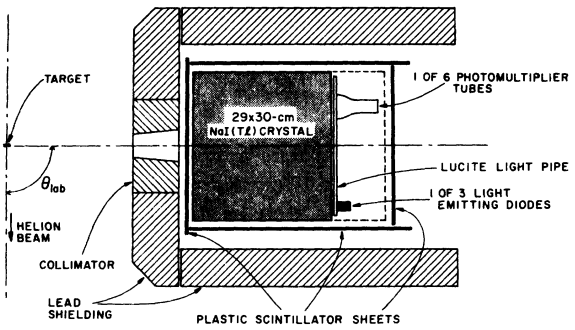


FIG. 1. Schematic illustration of the NaI(Tl) $\gamma$-radiation detector and its associated cosmic-ray anticoincidence shield. A horizontal cross section is shown. Four of the six plastic scintillator sheets comprising the anticoincidence shield may be seen in this cross section. For simplicity, their light pipes and phototubes are not also drawn.

The effective detection solid angle was thus determined with an accuracy of better than 1%. The remaining four lead walls served to reduce background $\gamma$ radiation. The NaI(Tl) crystal was completely surrounded by a six-sided box comprising six separate thin (0.32-cm-thick) plastic scintillator sheets, four of which are shown in the horizontal cross section, Fig. 1. Each of these scintillators was optically coupled to a fast, high-gain phototube (Amperex 56 DVP) via a low-loss adiabatic light pipe (thin Lucite strips which were bonded to one edge of the scintillator and which were gradually twisted to form a bundle). The passage of a cosmic-ray muon through the NaI crystal triggered at least two plastic-scintillator panels. A fast coincidence (15–30 ns) between at least two of the plastic-scintillator sheets thus served to veto any coincident signal from the NaI(Tl) crystal. Some 95% of all cosmic-ray events depositing 20–40 MeV in the NaI(Tl) crystal were rejected by this technique. The measured trigger efficiency for a muon transversing one panel is better than 99.85%, but roughly 5% of the cosmic-ray muons stopped in the crystal and failed to trigger a second panel. Because of the small scintillator volume and because of the fast twofold coincidence requirement, less than 0.2% of the valid $\gamma$ events were erroneously rejected under operating conditions in which the total counting rate in the NaI(Tl) crystal exceed $2 \times 10^5$ sec. This approach represents then a compromise which sacrifices efficiency of cosmic-ray rejection (95% in contrast to 99.7% cited by Diener *et al.*[16]) to gain insensitivity to the neu-

tron background. This anticoincidence shield is discussed in greater detail by Shay.[20]

Also indicated in Fig. 1 are three gallium phosphide light-emitting diodes (LED's) which were optically coupled to the phototubes viewing the crystal. These were pulsed at a rate proportional to the beam current. The signals driving the LED's were shaped so that their light flashes simulated the scintillations produced in the NaI(Tl) crystal. Our tests revealed that the amplitude of these signals drifted by no more than 0.5% in any 48-h period. The signals arising from the LED's were used to monitor and control both the gain drifts of the electronics and the electronic pileup during the experiment.

Since the principal factor determining the energy resolution is the intrinsic response of the NaI(Tl) crystal to high-energy $\gamma$ photons rather than the counting statistics of photoelectrons, the shortening of the anode signals by clipping may greatly reduce spectral distortion from pileup without concomitantly sacrificing resolution. The approach described below is similar to that taken as well by Kernel and Mason[9] and by Diener *et al.*[16]

The electronic instrumentation used in these experiments is diagramatically illustrated in Fig. 2. Signals from the dc-coupled photomultiplier tubes (Amperex XP 1031) viewing the NaI(Tl) crystal were first amplified in a fast dc-coupled amplifier and these clipped to roughly a 250-ns width by a delay line terminated to restore the zero base line. A high-level leading-edge fast dc-coupled discriminator opened a dc-coupled linear gate for a period of time just wider than the shaped pulse. Because the shaped pulse was short, it was improbable that two small signals could add together to result in a spurious gate opening, and because the gate opening was so narrow, only rarely would low-energy events be integrated along with valid high-energy events. Since the system was dc coupled from the phototubes to the analog-to-digital converter (ADC), the problem of base-line shifts was avoided. Under actual running conditions, resolution was not greatly impaired by clipping the signal to such a short length; Fig. 3 illustrates a $^{11}$B$(p,\gamma)^{12}$C spectrum taken with a total counting rate of greater than $2.5\times10^5$/sec. Brassard[6,21] discusses this approach in greater detail, as well as the specific circuits constructed for use in this system.

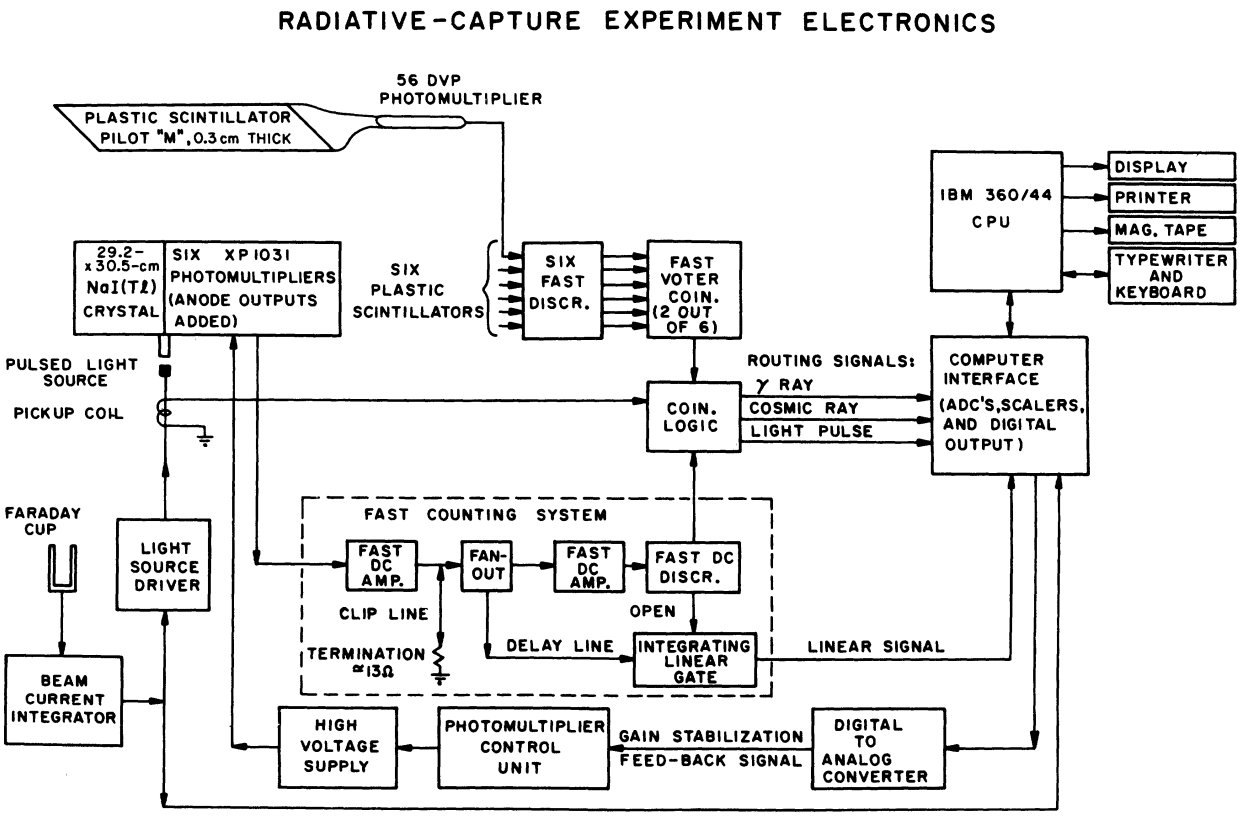


FIG. 2. Radiative-capture experiment electronics. For simplicity, only one of the six plastic scintillators is shown. The portion enclosed in the dashed box is termed the "fast counting system" in the text.

As is indicated in Fig. 2, the valid signals were routed by coincident logic signals to one of three spectra; the "$\gamma$-ray" spectrum of the reactions of interest, the "light-pulse" spectrum (the spectrum arising from the flashes of the LED's), and the "cosmic-ray" spectrum (the spectrum of signals rejected by the plastic-scintillator array). These signals were converted by an ADC and processed by an on-line IBM 360/44 computer. The centroid of the narrow LED peak was continuously monitored by the computer. Whenever drifts in this centroid were observed, the computer directed a compensatory change in the gain of the phototube via an ADC servoloop. In addition, continuous monitoring of the width of the LED peak provided an on-line estimate of pileup. The output of the beam-current integrator was scaled. The dead time of ADC, invariably very small because of the low valid-event count rate, was determined by the number of events routed to channel zero of the $\gamma$ spectrum. At the conclusion of each data-taking period, the spectra, along with pertinent information (e.g., the beam energy, the angle of the detector, and the integrated beam current) were written on magnetic tape.

### 3. DATA REDUCTION

Helion capture populated levels above 26.28 and 22.79 MeV in the compound systems of $^{12}$C and $^{16}$O, respectively. In these studies we detected the subsequent $\gamma$ decays (Figs. 4 and 5) to the low-lying states. The four transitions $\gamma_0$, $\gamma_1$, $\gamma_2$, and $\gamma_3$ proceeding to the ground state and first three excited states in $^{12}$C are all well resolved as the $^{9}$Be($^{3}$He, $\gamma$)$^{12}$C spectrum of Fig. 6 demonstrates. The discriminator threshold falls at channel 60 in this spectrum and is the cause of the peak appearing there. The first four excited states of $^{16}$O, however, have excitation energies 6.05, 6.13, 6.92, and 7.12 MeV so that these transitions are seen as two poorly resolved peaks in the $^{13}$C-($^{3}$He, $\gamma$)$^{16}$O spectrum of Fig. 7.

The pileup of low-energy events is seen in the two spectra as a background (roughly exponentially decreasing) upon which the peaks of the individual transitions are superposed. This background is far more pronounced, and troublesome, in the $^{13}$C($^{3}$He, $\gamma$)$^{16}$O spectrum because of the extremely intense 15.11-MeV transition resulting from the well-known reaction $^{13}$C($^{3}$He, $\alpha\gamma_{15.11}$)$^{12}$C. The 15.11-MeV state ($1^+$, 1) of $^{12}$C is bound for neutron and proton decay, and $\alpha$ emission is forbidden by conservation of isospin. As a consequence, the

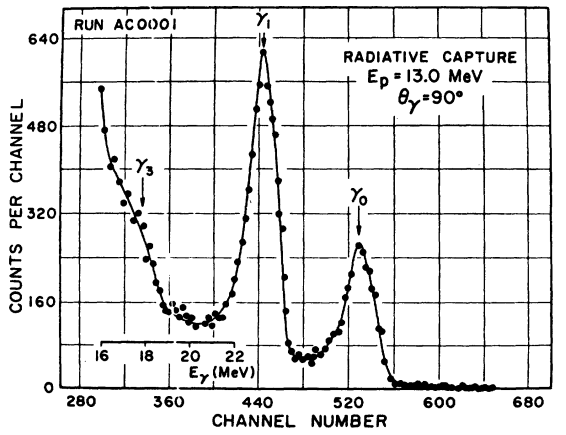


FIG. 3. $\gamma$-radiation spectrum of the reaction $^{11}$B($p$, $\gamma$)-$^{12}$C. This spectrum was taken with a total counting rate of roughly $2.5\times10^5$/sec. The lower half of the spectrum is below the discriminator threshold. The energy of the ground-state transition is roughly 28 MeV; the resolution of this transition is about ≃6% (full width at half maximum).

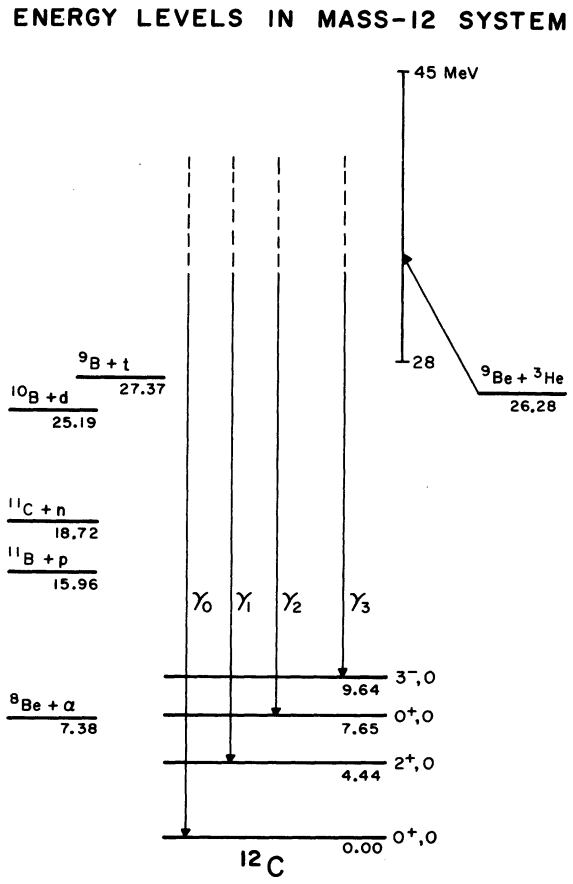


FIG. 4. Energy level diagram for $^{12}$C. The threshold for emission of a helion is 26.28 MeV. The excitation region investigated here is 28 to 45 MeV. The transitions to the ground state and the first three excited states are observed in this experiment.

cross section of this reaction is of the order of millibarns. The residual cosmic-ray background is generally insignificant as is attested by the appearance of the high-energy part of these spectra.

Each spectrum has been fitted with a sum of peaks plus an exponential background to account for pileup. The parametrized peak shapes for monochromatic $\gamma$ radiation are based on the observations of Bramblett *et al.*[22] These peak shapes, Gaussian with exponentially falling low-energy tails, are shown as the light lines in Fig. 8. By contrast, the actual data of these radiative-capture experiments are best fitted with peak shapes having a constant low-energy tail (the heavy lines in Fig. 8). The discrepancy between the two peak shapes may arise from a variety of processes in the radiative-capture experiments such as spectral distortion by residual high-low pileup mentioned by Diener *et al.*[16] We have fitted with the peak shapes depicted by the heavy lines, but have integrated only those counts lying

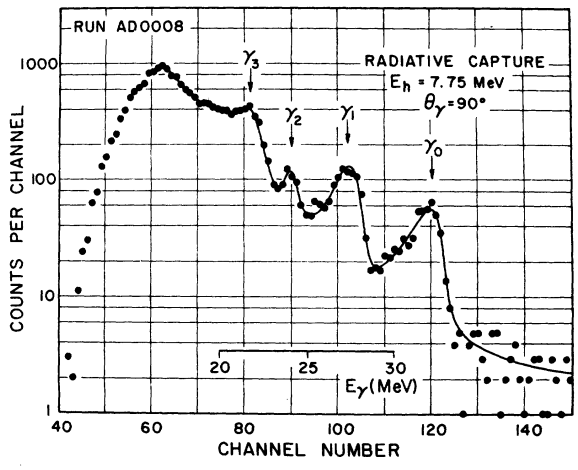


FIG. 6. $\gamma$-radiation spectrum for the reaction $^9$Be-($^3$He,$\gamma$)$^{12}$C. Each transition is denoted by $\gamma_i$. A calibration of the $\gamma$ energy is included. For energies higher than the $\gamma_0$ transition, only the residual cosmic-ray background is present.

beneath the light lines. This procedure is admittedly *ad hoc* and constitutes the chief uncertainty in the over-all normalization of the cross section reported here. During the fitting the only free parameters are the height and position of each peak and the two exponential background parameters. The parameters specifying the monochromatic $\gamma$ peak shapes (width, etc.) are not altered during the fitting; and, moreover, each sequence of spectra is fitted with the same peak shapes. The set of peak-shape parameters used

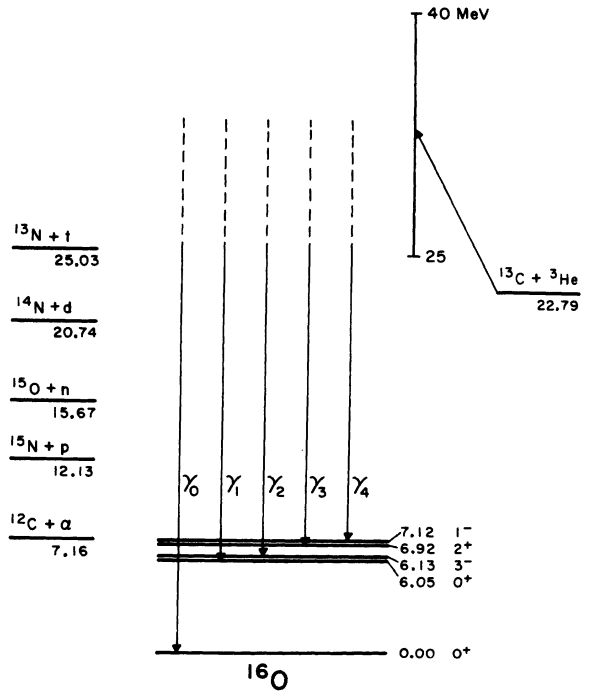


FIG. 5. Energy level diagram for $^{16}$O. The threshold for the emission of a helion is 22.79 MeV. The transition to the ground state is observed clearly, but the transitions to the first four excited states are not well resolved.

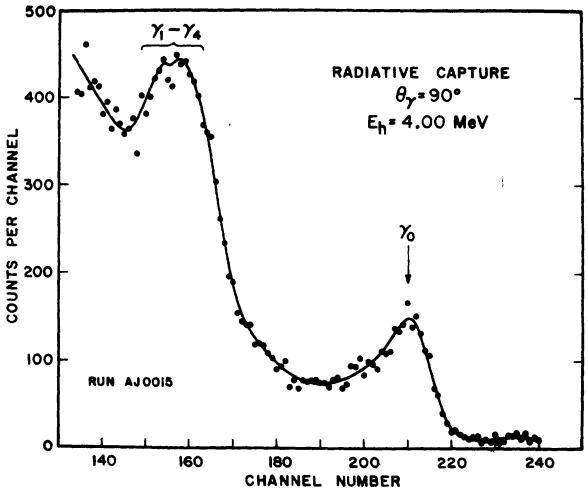


FIG. 7. $\gamma$-radiation spectrum for the reaction $^{13}$C-($^3$He,$\gamma$)$^{16}$O. The transitions to the first four excited states, $\gamma_1$–$\gamma_4$, are not resolved. The low-energy pileup tail is seen to extend even into the valley between $\gamma_0$ and $\gamma_{1-4}$.

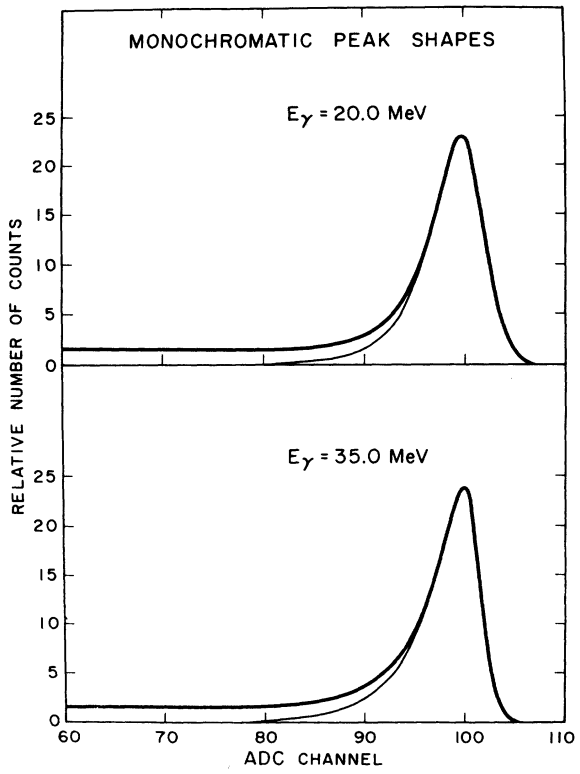


FIG. 8. Monochromatic $\gamma$-radiation peak shapes. The heavy line was used in fitting, while only the counts under the light line were integrated.

in fitting these spectra was determined by fitting a number of $^{11}B(p,\gamma)^{12}C$ spectra taken expressly for this purpose.

The fitting routine is a modified version of that written by Brassard for use on the Wright Nuclear Structure Laboratory (WNSL) IBM 360/44 computer and is described in detail in Ref. 6. In fitting the $^{9}Be(^{3}He,\gamma)^{12}C$ spectra, peaks for four transitions have been used throughout, except at very low helion energies where a transition to the 10.84-MeV state is also observed. Since the region of the spectrum considered in fitting does not extend more than several MeV below $\gamma_3$, the statistical errors of the $\gamma_3$ cross section and the exponential background are strongly coupled. As a consequence, the statistical errors associated with the $\gamma_3$ cross sections are much larger than those for the $\gamma_0$ or $\gamma_1$ cross sections. Likewise, the $\gamma_2$ transition falls between two much stronger transitions ($\gamma_1$ and $\gamma_3$) and has larger statistical errors than $\gamma_0$, whose cross sections are comparable. The fitted energies of the $\gamma_2$ and $\gamma_3$ transitions, however, consistently check (to better than 1%) with the correct $\gamma$ energies.

The $^{13}C(^{3}He,\gamma)^{16}O$ spectra were fitted two different ways. One fitting procedure used an exponential background plus one peak to represent the $\gamma_0$ transition; here, the fitting region extended only some 4 or 5 MeV below the $\gamma_0$ peak. In the other case, three peaks were used for the five $\gamma$ transitions: one for the $\gamma_0$ transition, one for $\gamma_1+\gamma_2$, and one for $\gamma_3+\gamma_4$. In these fits, the $\chi^2$ was determined from a region extending several MeV below the $\gamma_3+\gamma_4$ peak. Because the $\gamma_1+\gamma_2$ and $\gamma_3+\gamma_4$ peaks are not completely resolved, the cross section for either peak has fairly large statistical errors, and so we quote here only the cross sections for all four transitions, the sum of

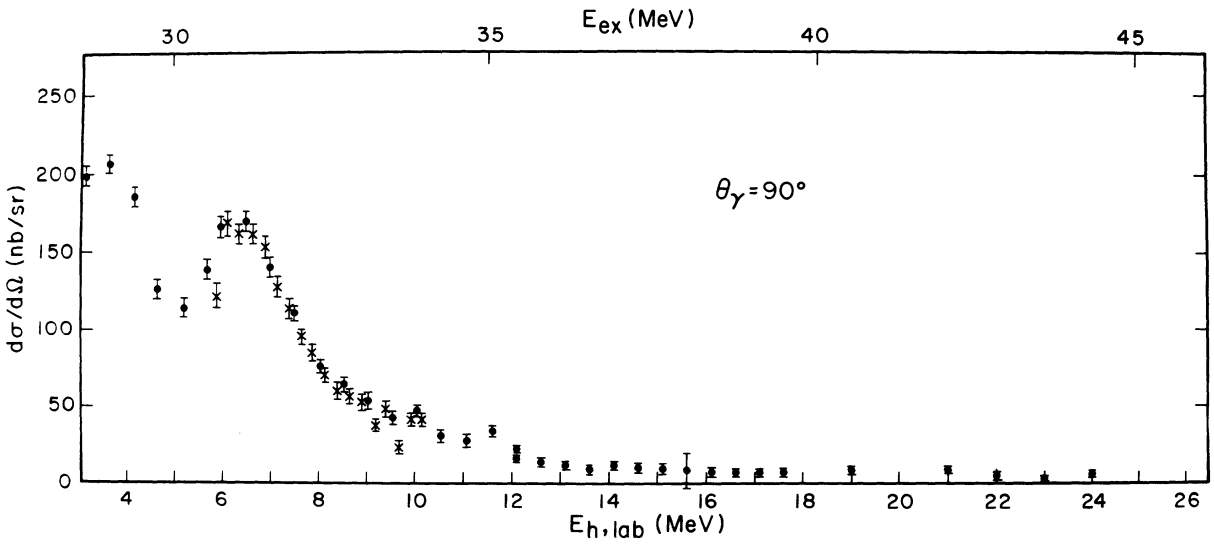


FIG. 9. 90° differential cross sections for the reaction $^{9}Be(^{3}He,\gamma_0)^{12}C$. Points represented by ×'s were obtained with a thinner target. Error bars include only statistical errors.

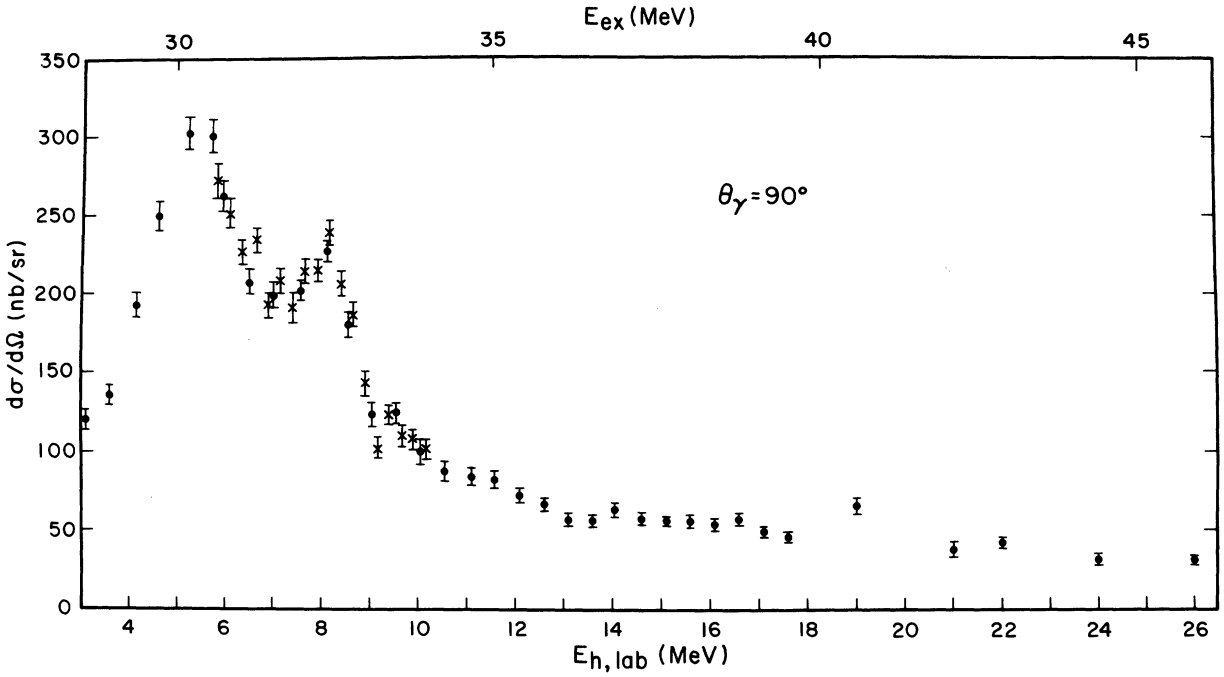


FIG. 10. 90° differential cross sections for the reaction $^9$Be($^3$He, $\gamma_1$)$^{12}$C. Points represented by ×'s were obtained with a thinner target. Error bars include only statistical errors.

$\gamma_1+\gamma_2$ and $\gamma_3+\gamma_4$. The values for $\gamma_0$ obtained by these two fitting procedures and those obtained by integrating "by hand" were all consistent.

All the statistical errors for differential cross sections may be found directly from the diagonal elements of the error matrix computed by our data analysis routine. The error bars shown on the excitation functions and the errors used in the Legendre polynomial fitting of the angular distributions are exclusively statistical.

Possible systematic errors may arise from several causes. The target thicknesses were determined by an $\alpha$-particle gauge whose reproducibility was certainly much better than 5%. As discussed by Barnes *et al.*,[19] however, the systematic uncertainty of this instrument is perhaps 10%. The greatest uncertainty in determining the number of incident helions was the electronic beam-current integrator itself; our tests revealed nonlinearities as great as 2–3%. The probably

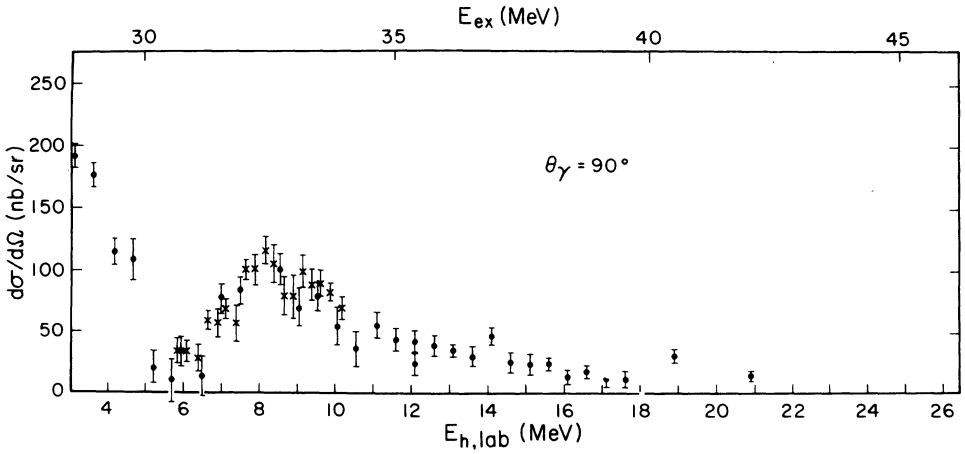


FIG. 11. 90° differential cross sections for the reaction $^9$Be($^3$He, $\gamma_2$)$^{12}$C. Points represented by ×'s were obtained with a thinner target. Error bars include only statistical errors.

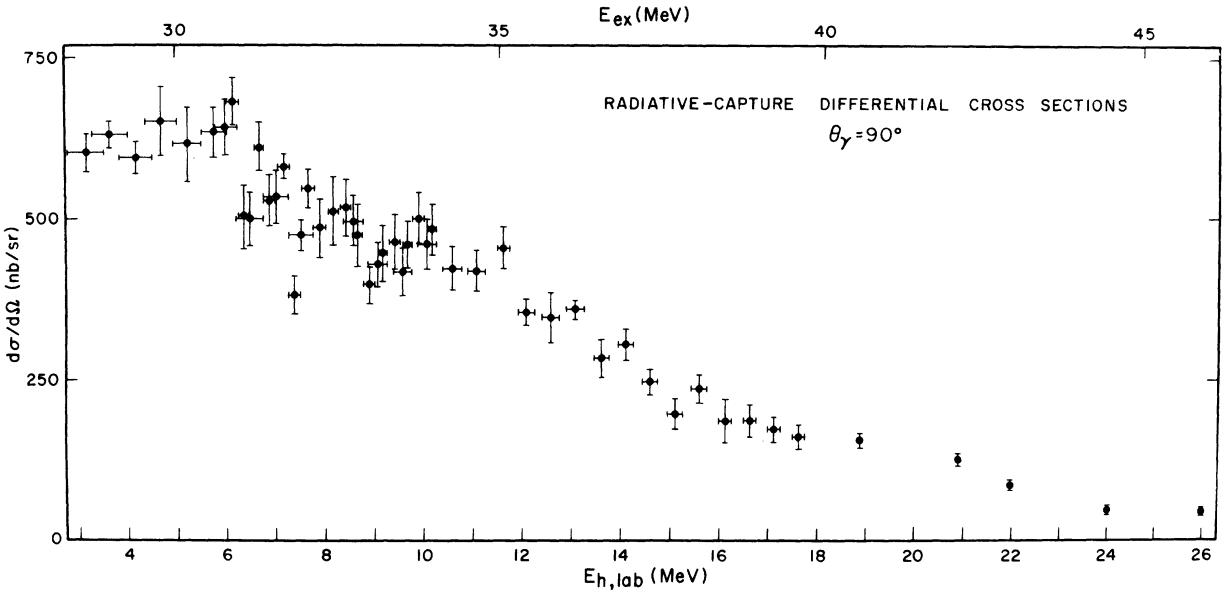


FIG. 12. 90° differential cross sections for the reaction $^{9}Be(^{3}He,\gamma_3)^{12}C$. The target thicknesses are indicated by the horizontal bars. Only statistical errors are included in the error bars.

systematic error in the determination of the solid angle was certainly less than 1%.

Most of the systematic errors discussed so far would be reflected in discrepancies between different sequences of data since several different targets, beam intensities, and detector positions were used. In angular distributions, data points were taken twice at $\theta_{lab} = 90°$ as a check on reproducibility. The several sets of data, however, corroborate one another to considerably better

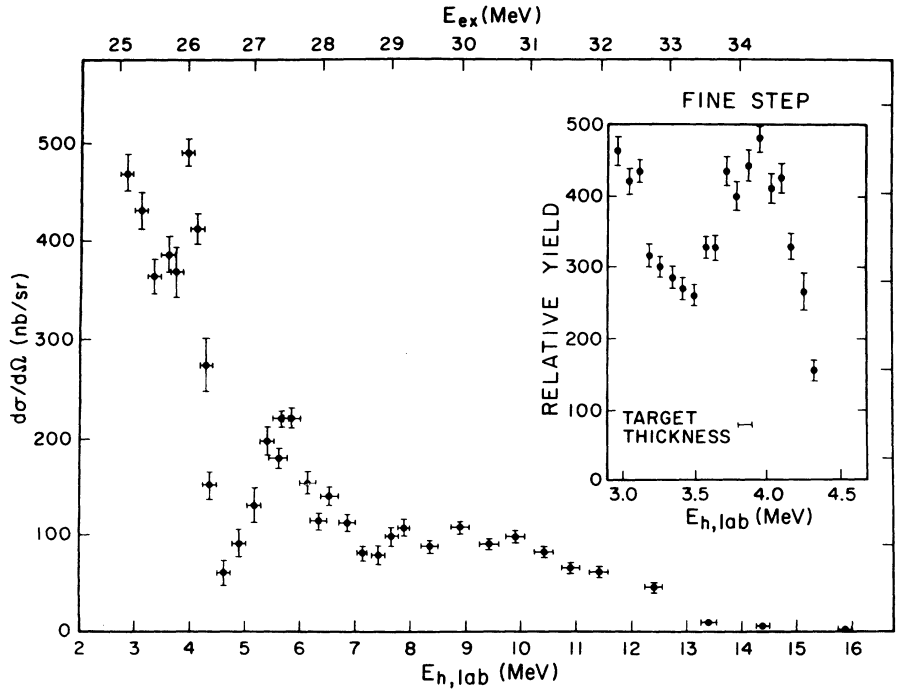


FIG. 13. 90° differential cross sections for the reaction $^{13}C(^{3}He,\gamma_0)^{16}O$. Errors assigned to the cross sections are wholly statistical. Horizontal bars represent the target thicknesses. The inset depicts a fine-step excitation function across the region of greatest structure, $3.0 < E_h < 4.5$ MeV; its ordinate is in relative units.

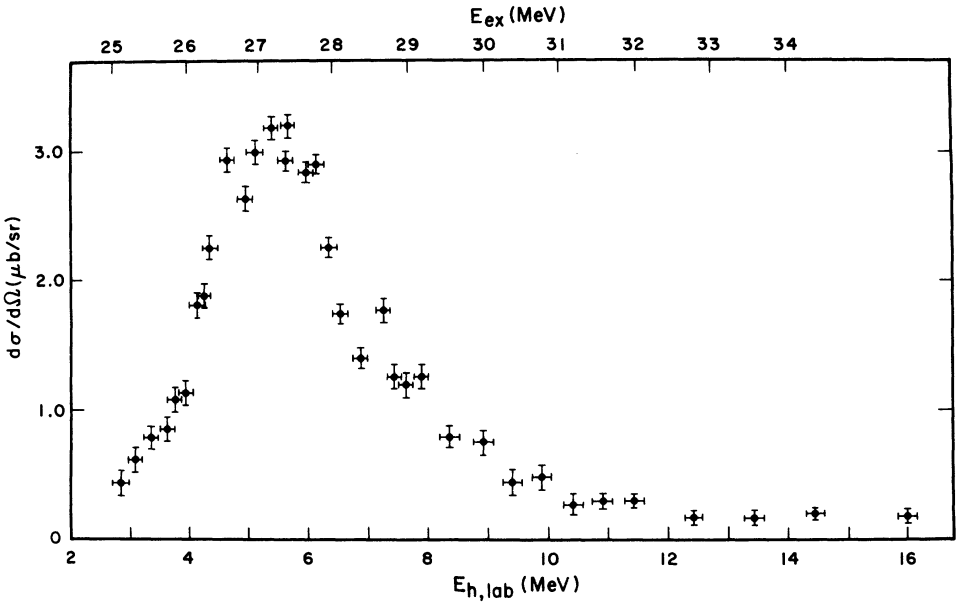


FIG. 14. 90° differential cross section for the reactions $^{13}$C($^3$He, $\gamma_{1-4}$)$^{16}$O. The cross sections of the four unresolved transitions are summed. Error bars represent statistical errors only. Horizontal bars signify the target thicknesses.

than 10%. The choice of monochromatic $\gamma$ peak shapes, on the other hand, constitutes a possible source of systematic error in the over-all absolute normalization. Only the normalization is affected since the difference between possible peak shapes changes little with $\gamma$ energy. As is discussed below, another choice of line shapes does result in extracted cross sections[23,24] uniformly greater than ours by a factor of 1.6.

Figures 9 through 12 depict the $^9$Be($^3$He, $\gamma$)$^{12}$C

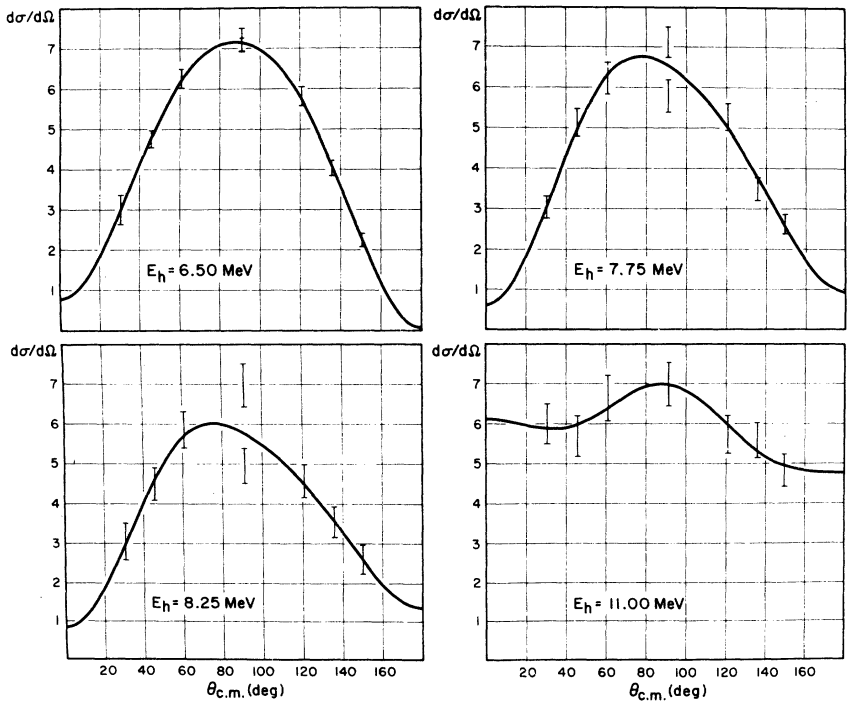


FIG. 15. Angular distributions of the reaction $^9$Be($^3$He, $\gamma_0$)$^{12}$C. Data are shown as bars, the height of which represents the statistical errors. The solid lines are Legendre polynomial fits, $d\sigma/d\Omega = \sum_{n=0}^{4} A_n P_n(\cos\theta_{c.m.})$. Units are arbitrary.

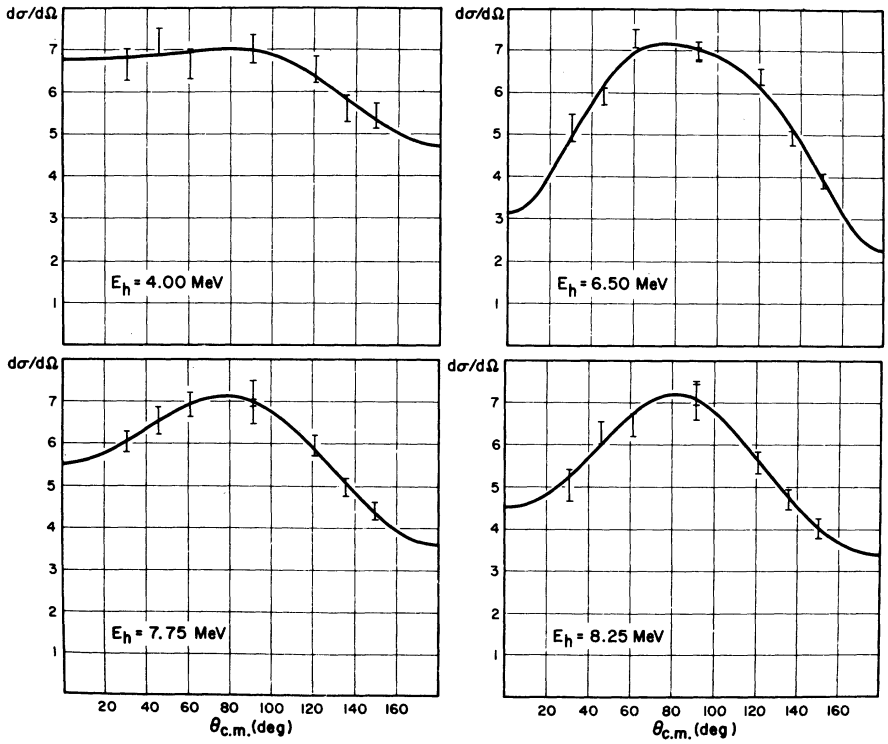


FIG. 16. Angular distributions of the reaction $^{9}$Be($^{3}$He, $\gamma_1$)$^{12}$C. Data are shown as bars, the height of which represents the statistical errors. The solid lines are Legendre polynomial fits, $d\sigma/d\Omega = \sum_{n=0}^{4} A_n P_n(\cos\theta_{c.m.})$. Units are arbitrary.

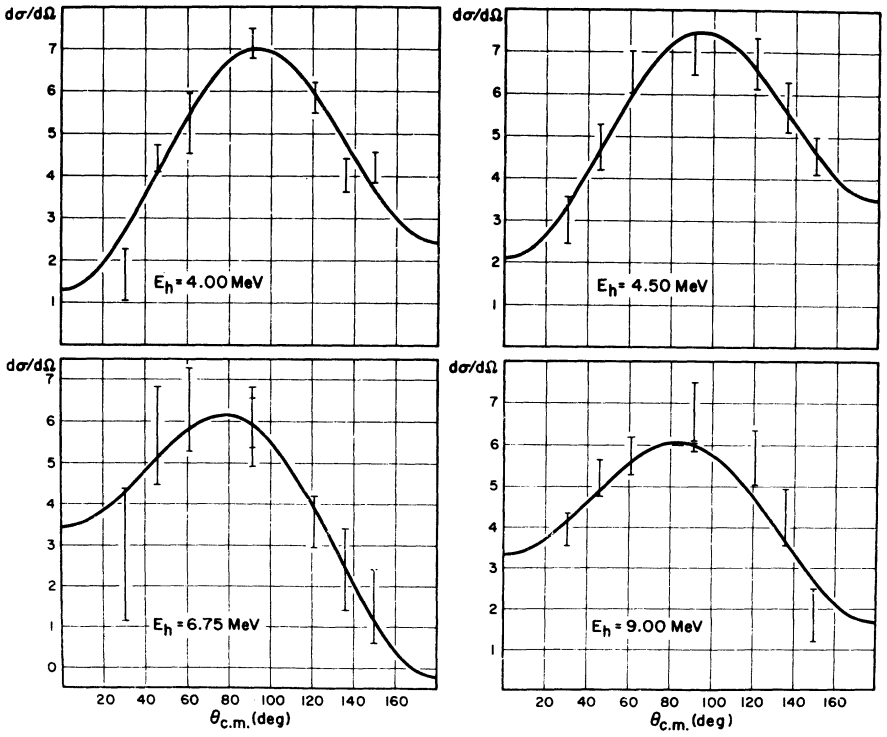


FIG. 17. Angular distributions of the reaction $^{9}$Be($^{3}$He, $\gamma_2$)$^{12}$C. Data are shown as bars, the height of which represents the statistical errors. The solid lines are Legendre polynomial fits, $d\sigma/d\Omega = \sum_{n=0}^{4} A_n P_n(\cos\theta_{c.m.})$. Units are arbitrary.

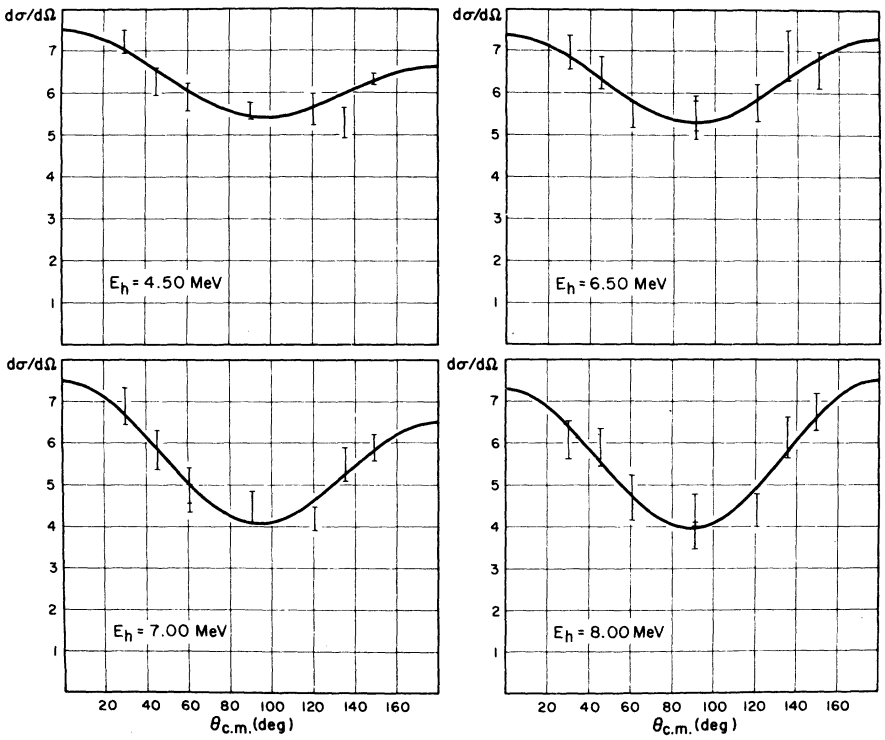


FIG. 18. Angular distributions of the reaction $^9$Be($^3$He,$\gamma_3$)$^{12}$C. Data are shown as bars, the height of which represents the statistical errors. The solid lines are Legendre polynomial fits, $d\sigma/d\Omega = \sum_{n=0}^{4} A_n P_n(\cos\theta_{c.m.})$. Units are arbitrary.

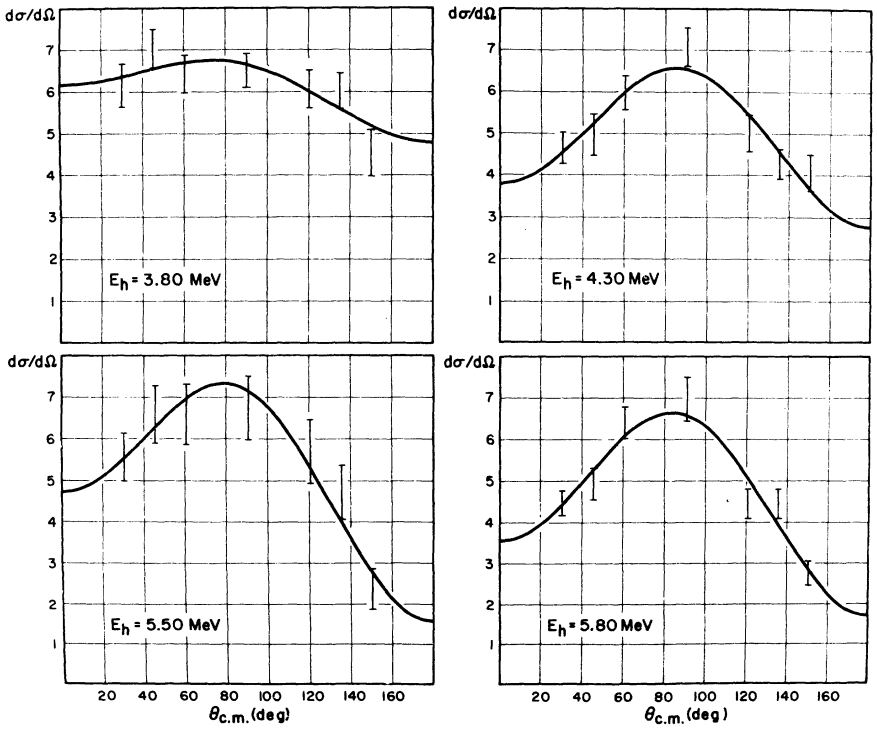


FIG. 19. Angular distributions of the reaction $^{13}$C($^3$He,$\gamma_0$)$^{16}$O. Data are shown as bars, the height of which represents the statistical errors. The solid lines are Legendre polynomial fits, $d\sigma/d\Omega = \sum_{n=0}^{4} A_n P_n(\cos\theta_{c.m.})$. Units are arbitrary.

90° excitation functions and Figs. 13 and 14, those of $^{13}C(^3He,\gamma)^{16}O$. The beam energy for each data point is the energy at the center of the target. In the $^9Be(^3He,\gamma)^{12}C$ experiment, sequences of data were taken with two different target thicknesses. In Figs. 9–11 the crosses represent the thinner target data whose thickness equals the spacing of these data points. In the other figures, target thicknesses are shown by error bars. The errors assigned to the differential cross sections in these figures are wholly statistical.

In the $^{10}Be(d,\gamma)^{12}C$ measurements no spectral peaks were observed. Rough estimates of the upper limits of the cross sections were made with a crude background subtraction. Over the energy range $E_x = 28$ MeV to $E_x = 33$ MeV, the 90° differential cross sections of $^{10}B(d,\gamma_0)^{12}C$ were less than 5 nb/sr and consistent with zero.

Differential cross sections of the helion radiative-capture reactions were measured at $\theta_{lab} = 30$, 45, 60, 90, 120, 135, and 150° for a large number of energies. Several typical angular distributions are shown in Figs. 15 through 20. Statistical errors are shown. The laboratory angle has been transformed into the center-of-mass system.

These angular distributions have been fitted with a sum of Legendre polynomials,

$$\frac{d\sigma}{d\Omega} = \frac{\sigma_T}{4\pi}\left[1 + \sum_\nu A_\nu P_\nu(\cos\theta)\right],$$

where $\sigma_T$ is the total cross section and $A_\nu$, the anisotropy coefficient for the $\nu^{th}$-order polynomial. The errors in $\sigma_T$ and the $A_\nu$'s are determined from the diagonal elements of the resulting error matrix and are only statistical since only the statistical errors of the differential cross sections were employed in their computation. Only the reactions $^9Be(^3He,\gamma_0)^{12}C$ and $^9Be(^3He,\gamma_1)^{12}C$ were measured to great enough precision to warrant fitting with orders up to $\nu = 4$, but only the anisotropy coefficients for $\nu = 1$ and 2 are significantly different from zero. In other reactions, the highest-order effective Legendre polynomial is that corresponding to $\nu = 2$. The fitted angular distributions are drawn as the solid lines in Figs. 15 through 20. The total cross sections and anisotropy coefficients are plotted as functions of energy (again, energy at the center of the target) in Figs. 21 through 26. The physically meaningful anisotropy coefficients are those measured with a point detector, and differential cross sections measured with a real detector are averaged over

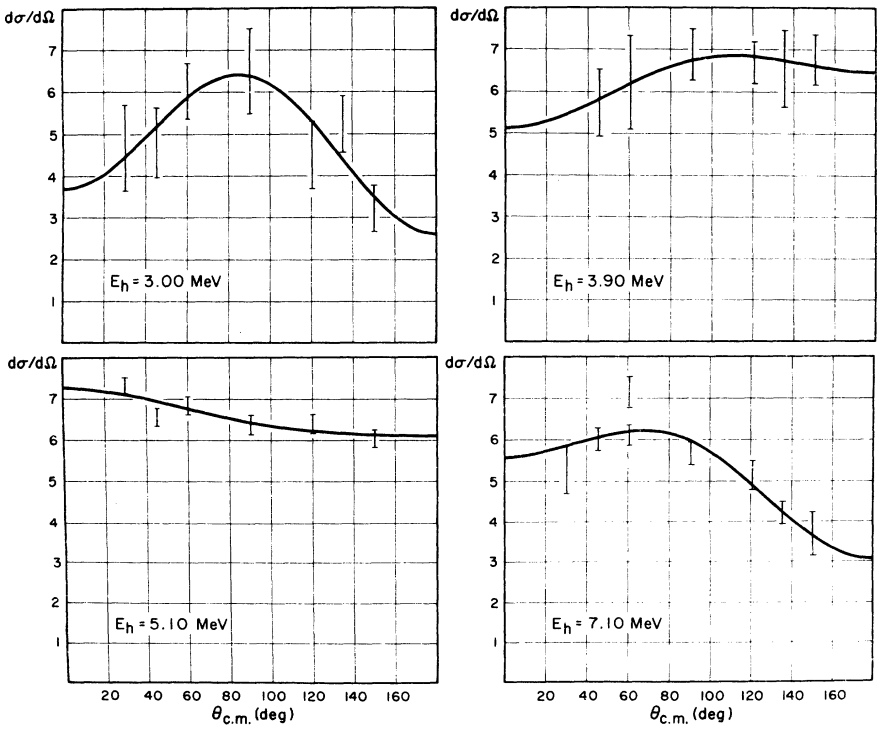


FIG. 20. Angular distributions of the reactions $^{13}C(^3He,\gamma_{1-4})^{16}O$. Data are shown as bars, the height of which represents the statistical errors. The solid lines are Legendre polynomial fits, $d\sigma/d\Omega = \sum_{n=0}^{4} A_n P_n(\cos\theta_{c.m.})$. Units are arbitrary.

its solid angle. The correction factors for the lower-order ($\nu=1$ and 2) anisotropy coefficients, however, are very nearly negligible.

## 4. DISCUSSION

Before considering the $R$-matrix calculation based on Wang and Shakin's wave functions in the light of these experimental results, we will first discuss these data in more general terms.

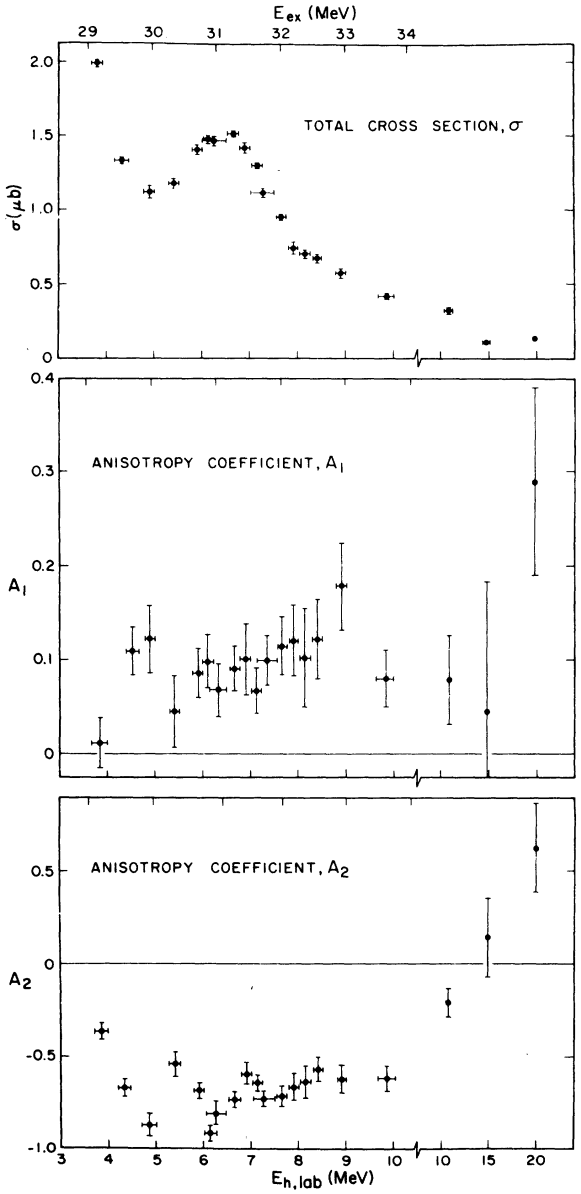


FIG. 21. Total cross section and anisotropy coefficients for the reaction $^9$Be($^3$He,$\gamma_0$)$^{12}$C. Shown are the results of fitting the $^9$Be($^3$He,$\gamma_0$)$^{12}$C angular distributions with $d\sigma/d\Omega = (\sigma/4\pi)[1+\sum_{i=1}^{4} A_i P_i(\cos\theta)]$. Errors are wholly statistical.

To obtain a crude parametrization of the 90° excitation functions, we have fitted these data with incoherent sums of Breit-Wigner forms

$$\sum_i \frac{A_i}{(E-E_i)^2+\frac{1}{4}\Gamma_i^2/4}.$$

Such a parametrization of differential cross sections is meaningful provided angular distributions do not change rapidly with energy; that is, when the 90° differential cross section reflects the energy dependence of the total cross section. Such a fitting procedure would be successful only if there were little interference between resonances and if there were little change in the helion pene-

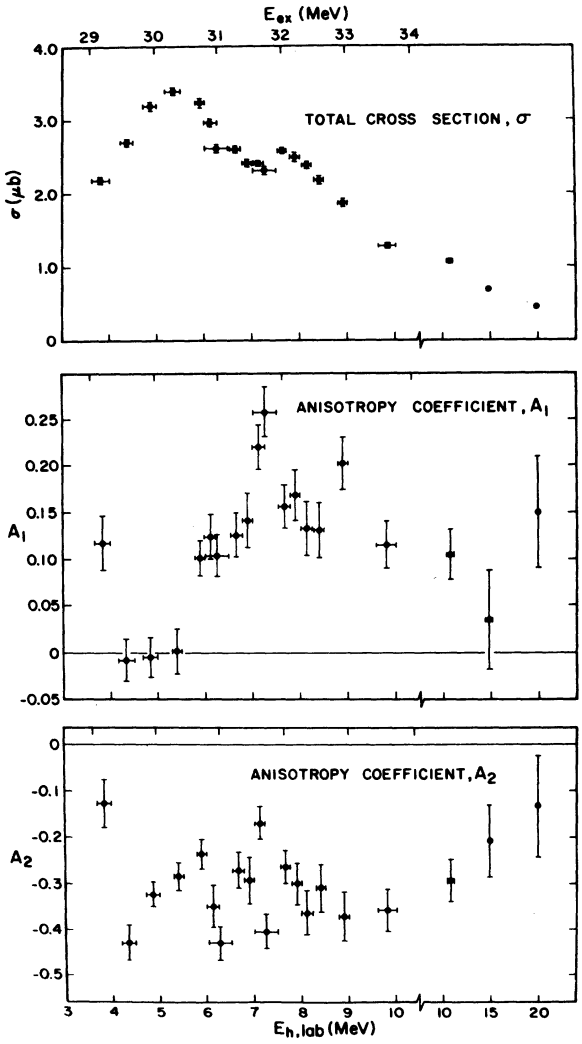


FIG. 22. Total cross section and anisotropy coefficients for the reaction $^9$Be($^3$He,$\gamma_1$)$^{12}$C. Shown are the results of fitting the $^9$Be($^3$He,$\gamma_1$)$^{12}$C angular distributions with $d\sigma/d\Omega = (\sigma/4\pi)[1+\sum_{i=1}^{4} A_i P_i(\cos\theta)]$. Errors are wholly statistical.

trability over the fitting region. For the reactions $^{9}$Be($^{3}$He, $\gamma_0$)$^{12}$C, $^{9}$Be($^{3}$He, $\gamma_1$)$^{12}$C, and $^{9}$Be($^{3}$He, $\gamma_2$)$^{12}$C this parametrization is found capable of describing the data quite well and the extracted resonance energies and widths are given in Table I. The resonance at $E_x = 28.83$ MeV is exhibited in both the $\gamma_0$ and the $\gamma_2$ decay; the 32.29- and 33.47-MeV resonances in both $\gamma_1$ and $\gamma_2$. The last resonance is rather broad and its identification, particularly in the $\gamma_1$ decay channel, where the resonance energy was constrained during fitting, is rather tenuous. The fact that this structure is present in several decay channels tends to support the supposition that the reactions are proceeding primarily via resonating states in the compound system. The fitting of the $^{13}$C($^{3}$He, $\gamma_0$)$^{16}$O data with Breit-Wigner shapes was notably less successful, principally because of the sharp interference dip at 26.6 MeV and the asymmetrical structure between 27.0 and 28.5 MeV. The experimental resonance energies and widths of the first two resonances ($E_x = 25.22 \pm 0.02$ and $25.96 \pm 0.05$ MeV with $\Gamma = 0.46 \pm 0.06$ and $0.53 \pm 0.06$ MeV, respectively) are, however, well determined by several fits.

If the observed $\gamma$ radiation were all electric dipole, then the measured angular distributions would be well described by the sum of only Legendre polynomials of orders 0 and 2. Interference between $E1$ and $M1$ radiation would result in a term of order 1, and interference between $E1$ and $E2$ would result in terms of orders 1 and 3. In practice, only the coefficients of the Legendre polynomials of orders 0, 1, and 2 are determined accurately, so the hallmark of interference $E1$ with either $E2$ or $M1$ radiation is the

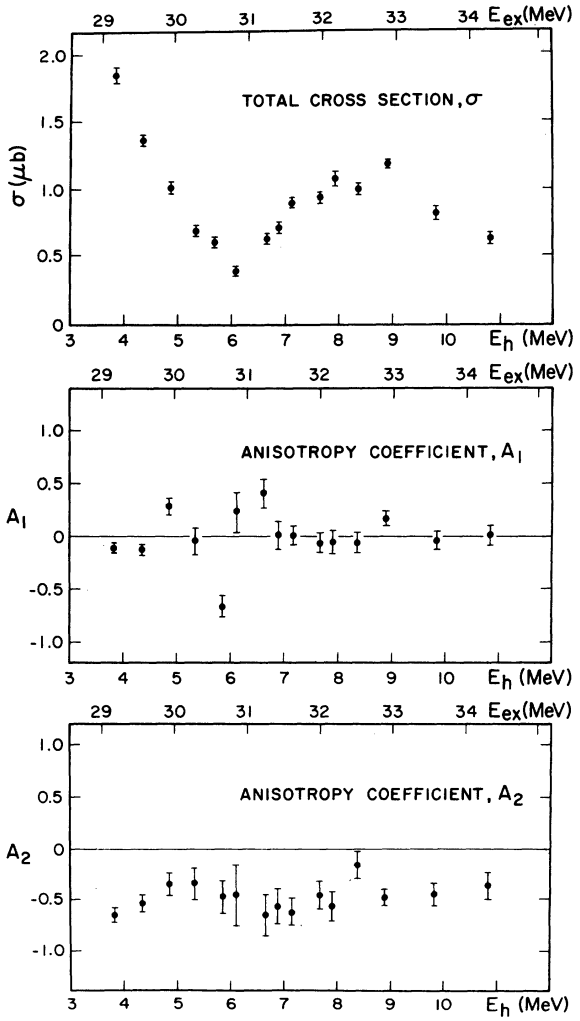


FIG. 23. Total cross section and anisotropy coefficients for the reaction $^{9}$Be($^{3}$He, $\gamma 2$)$^{12}$C. Shown are the results of fitting the $^{9}$Be($^{3}$He, $\gamma_2$)$^{12}$C angular distributions with $d\sigma/d\Omega = (\sigma/4\pi)[1 + \sum_{i=1}^{2} A_i P_i(\cos\theta)]$. Errors are wholly statistical.

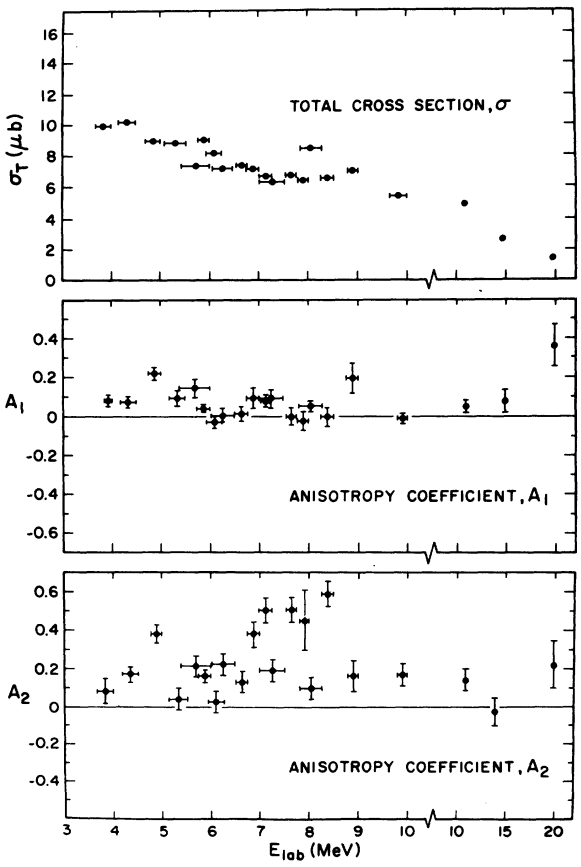


FIG. 24. Total cross section and anisotropy coefficients for the reaction $^{9}$Be($^{3}$He, $\gamma_3$)$^{12}$C. Shown are the results of fitting the $^{9}$Be($^{3}$He, $\gamma_3$)$^{12}$C angular distributions with $d\sigma/d\Omega = (\sigma/4\pi)[1 + \sum_{i=1}^{2} A_i P_i(\cos\theta)]$. Errors are wholly statistical.

detection of a significant $P_1$ term.

Using the Blatt and Biedenharn expression for differential cross sections given by Firk[25] and the tables compiled by Carr and Baglin[26], one obtains for the relative second-order Legendre polynomial coefficients of the $^9$Be($^3$He,$\gamma_0$)$^{12}$C angular distribution (with the assumption of an isolated intermediate $1^-$ state decaying only by $E1$ radiation)

$$A_2 = \frac{0.5 - 0.5b^2 + \sqrt{2}\,bc\cos\Delta}{1 + b^2 + c^2}\,, \qquad (1)$$

where $\Delta$ is the phase difference between the $s$ and $d$ partial waves (for channel spins $s=1$) and where $b$ and $c$ are the absolute values of the amplitudes of the $l=2$, $s=1$ and $l=0$, $s=1$ partial waves, respectively, relative to the $l=2$, $s=2$ partial waves. Even if the reaction were to proceed via such isolated intermediate states, the measurement of an angular distribution ($A_2$ coefficient) would not alone suffice to determine the three unknowns. In the limit $b \to \infty$ (all $d$ wave with channel spin $s=1$), $A_2 \to -5$. Toward lower energy, Coulomb and angular momentum barriers would tend to attenuate the $d$ partial waves first and result in an isotropic angular distribution such as we have observed experimentally. The behavior of the $^9$Be($^3$He,$\gamma_0$)$^{12}$C $A_2$ coefficient is thus consistent with predominately electric dipole radiation over the region of greatest interest. The slight departure from symmetry about 90° ($0. \leq A_1 \leq 0.10$) is consistent with a small $E1/M1$ interference. Since $E1/E2$ interference would here be characterized by a large $A_3$ coefficient, this possibility seems more remote.

Since the second excited state of $^{12}$C has $J^\pi = 0^+$, the relation (1) applies for $^9$Be($^3$He,$\gamma_2$)$^{12}$C also.

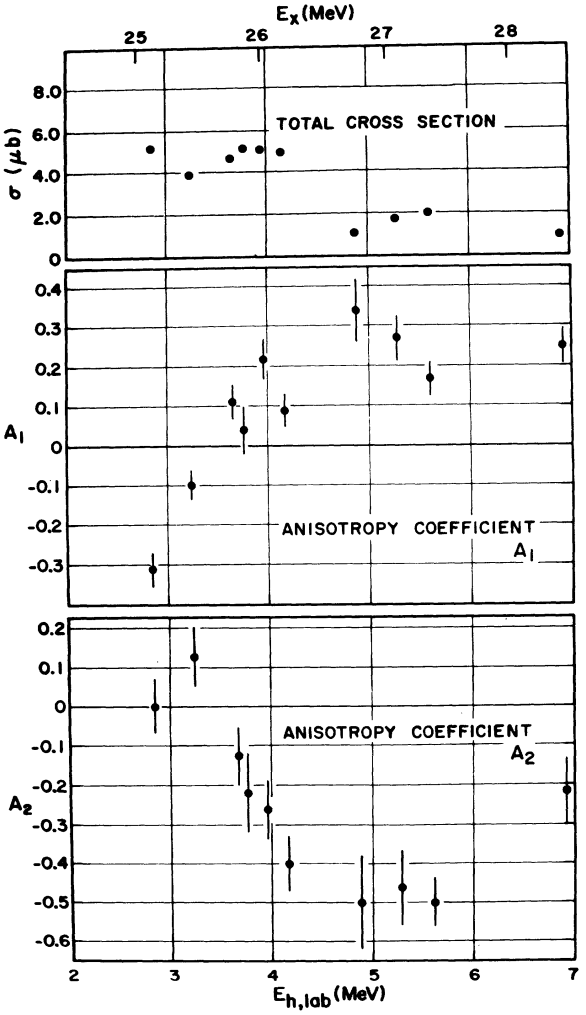


FIG. 25. Total cross section and anisotropy coefficients for the reaction $^{13}$C($^3$He,$\gamma_0$)$^{16}$O. Shown are the results of fitting the $^{13}$C($^3$He,$\gamma_0$)$^{16}$O angular distributions with $d\sigma/d\Omega = (\sigma/4\pi)[1 + \sum_{i=1}^{2} A_i P_i(\cos\theta)]$. Errors are wholly statistical.

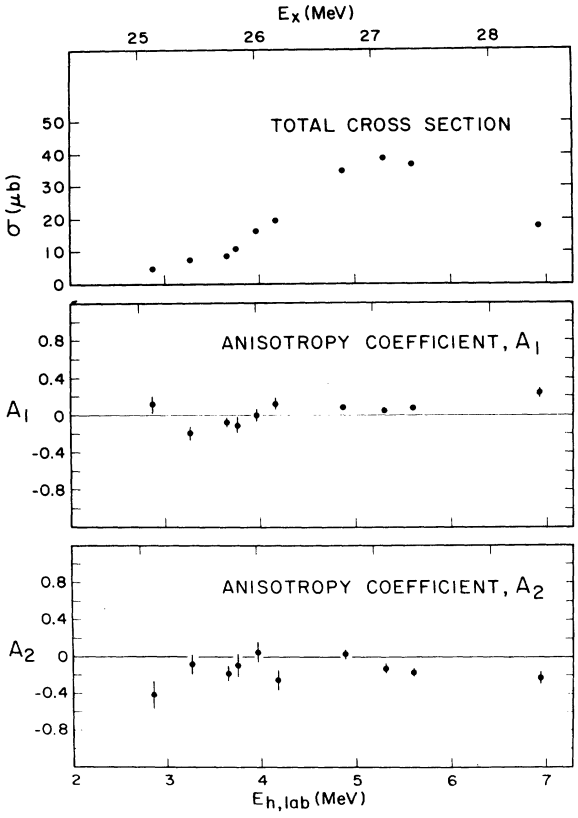


FIG. 26. Total cross section and anisotropy coefficients for the reactions $^{13}$C($^3$He,$\gamma_{1-4}$)$^{16}$O. Shown are the results of fitting the $^{13}$C($^3$He,$\gamma_{1-4}$)$^{16}$O angular distributions with $d\sigma/d\Omega = (\sigma/4\pi)[1 + \sum_{i=1}^{2} A_i P_i(\cos\theta)]$. Errors are wholly statistical.

TABLE I. Levels identified in $^{12}C$. Experimental energies and widths extracted from $^{9}Be(^{3}He,\gamma)^{12}C$ excitation functions. The resonance parameters for each of the three decays, $\gamma_0$, $\gamma_1$, $\gamma_2$, are listed separately and, for those resonances appearing in several decays, the combined values are given. All values are in MeV.

| Combined | | $\gamma_0$ decay | | $\gamma_1$ decay | | $\gamma_2$ decay | |
|---|---|---|---|---|---|---|---|
| $E$ | $\Gamma$ | $E$ | $\Gamma$ | $E$ | $\Gamma$ | $E$ | $\Gamma$ |
| 28.83±0.04 | 1.54±0.09 | 28.84±0.04 | 1.55±0.09 | ... | ... | 28.78±0.07 | 1.19±0.44 |
| 30.29±0.03 | 1.96±0.15 | ... | ... | 30.29±0.03 | 1.96±0.15 | ... | ... |
| 31.16±0.03 | 2.10±0.15 | 31.16±0.03 | 2.10±0.15 | ... | ... | ... | ... |
| 32.29±0.04 | 1.32±0.23 | ... | ... | 32.30±0.04 | 1.12±0.39 | 32.22±0.11 | 1.43±0.29 |
| 33.47±0.21 | 1.93±0.05 | ... | ... | 33.47 | 2.03±0.06 | 33.47±0.21 | 1.82±0.11 |

The measured $A_2$ coefficient is roughly −0.50 in the range $29 < E_x < 34$ MeV and within errors $A_1$ is zero. This decay is apparently dominated by $E1$ radiation. Because $E1$ decays to the first excited states ($J^\pi = 2^+$) may proceed from states of $J^\pi = 1^-$, $2^-$, or $3^-$, a relation analogous to (1) is too complicated to be enlightening. That the corresponding $A_2$ coefficient ($-0.45 \leq A_2 \leq -0.25$) is generally much larger than $A_1$, however, does attest to the role of electric dipole radiation. The $A_1$ coefficient is generally positive and, particularly for $31 \leq E_x \leq 33$ MeV, significantly greater than zero ($0.15 \leq A_1 \leq 0.25$), connoting appreciable $E1/M1$ or $E1/E2$ interference in this region. Since the 32.29- and 33.47-MeV resonances are common to both the $\gamma_1$ and $\gamma_2$ decays, it is improbable that either is a positive-parity state and is responsible for this peak in the $A_1$ coefficient observed in the $^{9}Be(^{3}He,\gamma_1)^{12}C$ reaction.

The $A_1$ and $A_2$ coefficients from fits of the angular distributions of $^{13}C(^{3}He,\gamma_0)^{16}O$ with Legendre polynomials $P_0$, $P_1$, and $P_2$ are shown in Fig. 25. The $A_1$ coefficient is large and exhibits a steady variation from −0.30 to 0.30. This striking be-

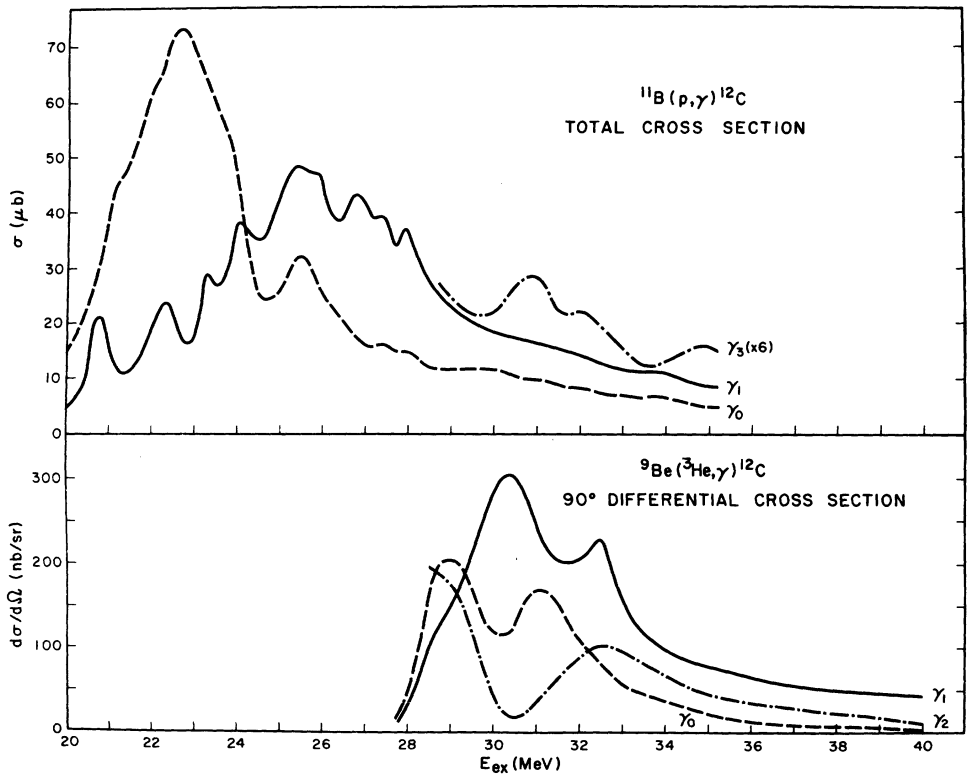


FIG. 27. Comparison of $^{12}C$ radiative-capture experiments. Above 29 MeV the $^{11}B(p,\gamma)^{12}C$ data are those of Brassard *et al.* (Ref. 6). Below 29 MeV the data are those of Allas *et al.* (Ref. 7) normalized to Brassard's data. The $^{9}Be(^{3}He,\gamma)^{12}C$ data are ours (above 28.5 MeV) and J. L. Black, G. A. Jones, and P. B. Treacy [Nucl. Phys. 54, 689 (1964)] (below 28.5 MeV).

havior in the $A_1$ coefficient suffices to confirm large $E2$ or $M1$ contributions. The $A_2$ coefficient first becomes positive and then falls to approximately $-0.50$ at 27.67 MeV. At 28.92 MeV, the value of the $A_2$ coefficient has risen back to $-0.20$. This variation in $A_2$ cannot easily be explained by such mechanisms as the energy dependence of penetrabilities. Were all the radiation $E1$, then $A_2$ would be $-0.5\,(-\delta\cos\Delta/\sqrt{2}+\delta^2)(1+\delta^2)^{-1}$ where $\delta$ is the ratio of the absolute value of the $s$ and $d$ partial-wave amplitudes (channel spin $s=1$) and $\Delta$ is their phase difference. For pure $s$-wave capture, the $A_2$ coefficient would then be zero. Despite the fact that the penetrability ratio $P_2/P_1$ varies sharply with energy, the predicted $A_2$ coefficients would not vary strongly enough with energy to account for the observed behavior.

Several interesting points arise from a comparison of these experiments with other radiative-capture work. The $^9$Be($^3$He, $\gamma_{0,1,2}$)$^{12}$C data of Blatt, Moon, and Kohler[27] ($1.0 \leq E_{\rm lab} \leq 6.0$) and of Linck and Kraus[28] ($1.5 \leq E_{\rm lab} \leq 11$ MeV) exhibit the same structure seen in our data over the same energy range. While the excitation functions of $^9$Be($^3$He, $\gamma_{0,1,2}$)$^{12}$C exhibit considerable structure in the range $27 < E_x < 34$ MeV, the $^{11}$B($p$, $\gamma_{0,1}$)$^{12}$C show only a slow monotonic decrease (Fig. 27). As well, the $^{12}$C($\gamma$, $n_0$)$^{11}$C data of Wu, Firk, and Phillips[12] contrasts with this helion-capture data and has much the same energy dependence as the proton capture.

As suggested by the $R$-matrix calculation of Brassard *et al.*,[6] the proton radiative capture in this region is largely dominated by the tails of several resonances in the giant-resonance region, 22–25 MeV for $\gamma_0$ and 24–28 for $\gamma_1$. States resonating in helion capture and having small proton widths then would scarcely affect the $^{11}$B+$p$ yield curves. Despite these differences the $\gamma_0$ and $\gamma_1$ decays in both radiative captures share nearly equal average branching ratios. Table II indicates $r_{11} = 1.75$ for proton capture and $r_{21} = 1.64$ for helion capture (the ratios $r_{11}$ and $r_{21}$ are defined in Table II). Quite possibly, then, helion capture populates states whose radiative decay proceeds by relatively simple configurations. In this view, the capture process occurs via 3p-3h configurations while the $\gamma$-decay transition proceeds through configurations simply related to the low-lying residual states—e.g., 1p-1h for a closed-core ground state. These mediating configurations might be those responsible for most of the $(\gamma, p)$ and $(\gamma, n)$ strength, even though no structure is seen in those yield curves.

By contrast, the decays to the second and third excited states are relatively very much stronger in helion capture than in proton capture. Table II indicates that $r_{12} \leq 0.05$ and $r_{13} \leq 0.34$ for proton capture while for helion capture $r_{22} = 0.79$ and $r_{23} = 4.73$, so that the relative enhancements for $\gamma_2$ and $\gamma_3$ are $r_{22}/r_{12} \geq 16$ and $r_{23}/r_{13} \simeq 14$, respectively. Gillet[29] noted that both the $0^+$ 7.65-

TABLE II. Average cross section of radiative capture reactions in $^{12}$C and their ratios.

| Reaction | Energy range (MeV) | Average 90° differential cross section $\gamma_0$ decay | $\gamma_1$ decay | $\gamma_2$ decay | $\gamma_3$ decay |
|---|---|---|---|---|---|
| $^{11}$B($p$,$\gamma$)$^{12}$C | 20–28 [a] | 3.8 | 3.0 | $\cong$0.02 [b] | ··· |
| | 28–35 [c] | 0.93 | 1.63 | $\ll$0.18 | 0.32 |
| $^9$Be($^3$He,$\gamma$)$^{12}$C | 28–35 [d] | 0.11 | 0.18 | 0.087 | 0.53 |
| $^{10}$B($d$,$\gamma$)$^{12}$C | 28–33 [d] | <0.003 | <0.005 | ··· | ··· |

Ratios of cross sections over the energy interval 28–35 MeV

$$r_1 \equiv \frac{\sigma[^9\mathrm{Be}(^3\mathrm{He},\gamma_0)^{12}\mathrm{C}]}{\sigma[^{11}\mathrm{B}(p,\gamma_0)^{12}\mathrm{C}]} = 1/11.8 \qquad r_{13} \equiv \frac{\sigma[^{11}\mathrm{B}(p,\gamma_3)^{12}\mathrm{C}]}{\sigma[^{11}\mathrm{B}(p,\gamma_0)^{12}\mathrm{C}]} = 0.34$$

$$r_2 \equiv \frac{\sigma[^{10}\mathrm{B}(d,\gamma_0)^{12}\mathrm{C}]}{\sigma[^{11}\mathrm{B}(p,\gamma_0)^{12}\mathrm{C}]} \cong 1/300 \qquad r_{21} \equiv \frac{\sigma[^9\mathrm{Be}(^3\mathrm{He},\gamma_1)^{12}\mathrm{C}]}{\sigma[^9\mathrm{Be}(^3\mathrm{He},\gamma_0)^{12}\mathrm{C}]} = 1.64$$

$$r_{11} \equiv \frac{\sigma[^{11}\mathrm{B}(p,\gamma_1)^{12}\mathrm{C}]}{\sigma[^{11}\mathrm{B}(p,\gamma_0)^{12}\mathrm{C}]} = 1.75 \qquad r_{22} \equiv \frac{\sigma[^9\mathrm{Be}(^3\mathrm{He},\gamma_2)^{12}\mathrm{C}]}{\sigma[^9\mathrm{Be}(^3\mathrm{He},\gamma_0)^{12}\mathrm{C}]} = 0.79$$

$$r_{12} \equiv \frac{\sigma[^{11}\mathrm{B}(p,\gamma_2)^{12}\mathrm{C}]}{\sigma[^{11}\mathrm{B}(p,\gamma_0)^{12}\mathrm{C}]} \leq 0.05 \qquad r_{23} \equiv \frac{\sigma[^9\mathrm{Be}(^3\mathrm{He},\gamma_3)^{12}\mathrm{C}]}{\sigma[^9\mathrm{Be}(^3\mathrm{He},\gamma_0)^{12}\mathrm{C}]} = 4.73$$

[a] Data of Allas *et al.* (Ref. 7) normalized to those of Brassard (Ref. 6) by factor of 1/1.6.
[b] Data of P. Paul, private communication.
[c] Data of Brassard (Ref. 6).
[d] This work.

MeV and $3^-$ 9.64-MeV states appear to be complex states not well suited to any 1p-1h description. Brassard *et al.* found that $^{11}B(p,\gamma_3)^{12}C^*$ cross sections predicted by a set of pure 1p-1h wave functions typically exceed the measured values by a factor of 5—a point which substantiates Gillet's conjecture. Furthermore, the analysis of Cohen and Kurath[30] has tentatively identified the $0^+$ 7.65-MeV state as $(2s1d)^2$, a 2p-2h state. As was pointed by Blatt, Moon, and Kohler,[27] if these strong $\gamma_2$ and $\gamma_3$ decays proceed mainly by 3p-3h → 2p-2h or by 3p-3h → 4p-4h, then the configurations responsible for the radiative decay might well be those with large helion-capture widths—that is, the 3p-3h components.

The observation of the 28.83-MeV resonance in both $\gamma_0$ and $\gamma_2$ decay channels may prompt an alternative view. The ground state might have a small, but significant 2p-2h admixture (the ground-state correlation predicted by Aggassi, Gillet, and Lumbruso[31] has a squared amplitude of 0.19) and the $0^+$ 7.65-MeV state might then contain a comparable admixture of 0p-0h configuration—the closed $p_{3/2}$ core. Such a picture, suggested by a similar model of Obst, Rauch, and Wahsweiler[32] for $^{90}Zr$, envisions $\gamma_0$ and $\gamma_2$ decays, particularly for the common resonance at 28.83 MeV, proceeding by both 1p-1h → core and 3p-3h → 2p-2h processes. The relative importance of decays via mediating 1p-1h configurations and decay directly from 3p-3h to 2p-2h cannot be easily estimated for either the $\gamma_0$ or $\gamma_2$ transitions.

The most striking contrasts provided in Table II are the relative $\gamma_0$ yields of the three radiative-capture reactions, $^{11}B+p$, $^9Be+{}^3He$, and $^{10}B+d$; 1.0, 0.085, and 0.0033, respectively. These ratios do not directly elucidate the nuclear structure of this excitation range since $E1$ radiation is forbidden in the case of deuteron capture to the extent that the isospin of the $1^-$, 1 highly excited levels is pure. Wu, Firk, and Phillips,[12] estimate [on the basis of the ratio of $(\gamma,n_0)$ and $(\gamma,p_0)$ cross sections] the amplitude of $T=0$ admixtures certainly to be less than 0.15 for this excitation

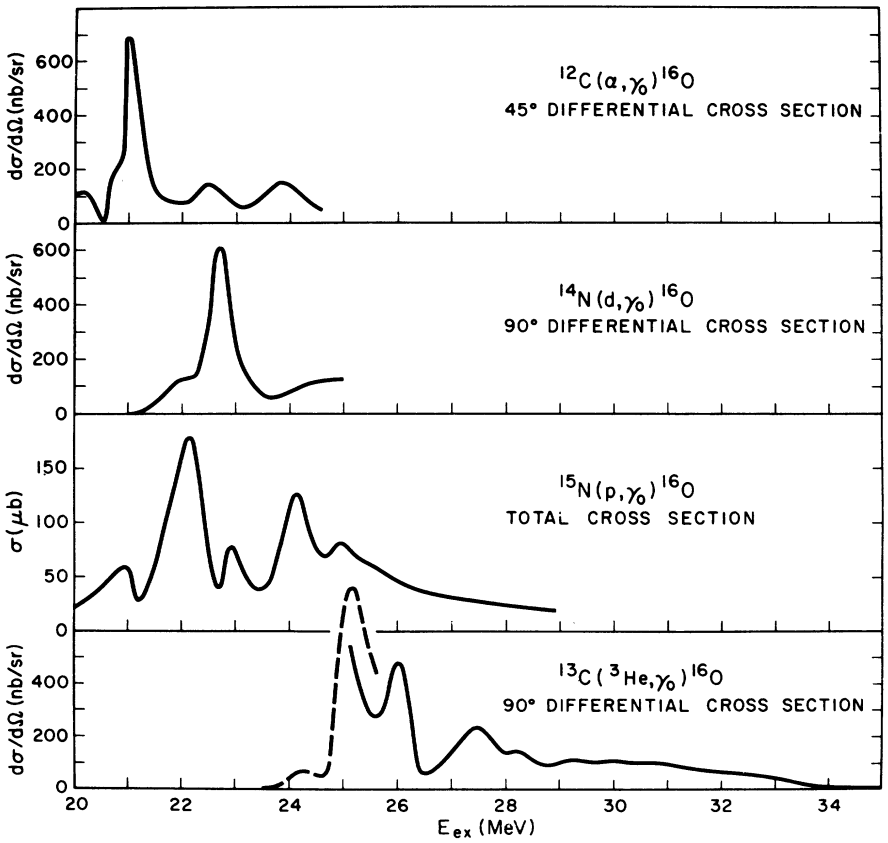


FIG. 28. Comparison of $^{16}O$ radiative-capture experiments. The $^{12}C(\alpha,\gamma_0)^{16}O$ data are those of Suffert and Feldman (Ref. 44); the $^{14}N(d,\gamma_0)^{16}O$, Suffert's (Ref. 42). O'Connell's $^{15}N(p,\gamma_0)^{16}O$ data (Ref. 11) have not been normalized by the factor of 1/1.6 required to achieve agreement with those of Earle and Tanner (Ref. 10). Likewise, Puttaswamy's (Ref. 23) data (dashed line) have not been normalized by the factor of 1/1.6 to correspond to our data (solid line).

range; this implies that, were all other factors the same, $^{10}B(d,\gamma_0)^{12}C$ would be inhibited with respect to $^9Be(^3He,\gamma_0)^{12}C$ some 45-fold. The experimental ratio of average cross sections is $\geq 33$ and thus completely consistent with this generous estimate of isospin mixing. One expects that, in addition to isospin inhibition, the reaction $^{10}B(d,\gamma_0)^{12}C$ also suffers structural inhibition. Whereas the three nucleons of an incident helion may be captured into $2s$-$1d$ orbits to form $1^-$, 1 states, the two nucleons of a captured deuteron must enter orbits of different parity in order to populate a state of negative parity.

Another experiment which has bearing on resonances observed here is the triton stripping reaction $^9Be(^7Li,\alpha)^{12}B$, which populates only $T=1$ states (in a neighboring $A=12$ nucleus). The triton stripping data of Glukhov *et al.*[33] imply strong feeding of states of excitation 13.60 and 15.25 MeV in $^{12}$B which correspond to excitations of 28.81 and 30.46 MeV in $^{12}$C (using the 15.21-MeV nuclear energy shift given by Ajzenberg-Selove[34]). The exceptionally close correspondence between these energies and those extracted for the lowest resonances observed in $^9Be(^3He,\gamma_{0,1,2})^{12}C$, 28.82 and 30.29 MeV, implies that these two states of large three-particle widths in $^{12}$B may be analogs of the two in $^{12}$C. This correspondence further substantiates a claim of resonant capture and radiative decay through relatively isolated states. Unfortunately, the Kurchatov group did not have a beam sufficiently energetic to investigate higher-lying levels in $^{12}$B.

The preliminary $^{13}C(^3He,\gamma_0)^{16}O$ excitation functions of Ventura *et al.*[24] corroborate our results except for a difference in normalization. The principal contrast to the $^{13}C(^3He,\gamma)^{16}O$ excitation functions is provided by those of $^{15}N(p,\gamma)^{16}O$ and $^{16}O(\gamma,n_0)^{15}N$. The third graph of Fig. 28 depicts the $^{15}N(p,\gamma_0)^{16}O$ of O'Connell[11]; the $^{16}O(\gamma,n_0)^{15}O$ results of Wu, Firk, and Phillips[12] are quite similar. Both O'Connell's data and the $^{13}C(^3He,\gamma_0)$-$^{16}O$ data of Puttaswamy[23] (the dashed line in Fig. 28) are illustrated without being reduced by a factor of 1.6 discussed earlier, the normalization difference presumably arising from a different choice of $\gamma$ peak shapes. O'Connell's total cross sections are characteristically 160 to 180% of those of Earle and Tanner.[10] The difference in normalization between our $^{12}$C data and those of Blatt, Moon, and Kohler,[27] probably also stems from a difference in choice of monochromatic $\gamma$ peak shape. The 25.22-MeV resonance observed in helion capture is well matched by the resonance occurring around 25.1 MeV in the 90° yield curve of Earle and Tanner[10] but which appears roughly at 24.9 MeV in O'Connell's work. It is more difficult to establish a correspondence between the 24.05-MeV resonance seen in the lower-energy helion-capture work of Puttaswamy and one in proton capture, observed at 24.3 MeV by Tanner and at 24.2 MeV by O'Connell but at 24.00 MeV by Wu, Firk, and Phillips[12] [in $(\gamma,n_0)$]. Puttaswamy favors designating two states, one seen at 24.3 MeV by proton capture and one seen at 24.05 MeV by helion capture. On the basis of Wu's data, however, we conclude that only one state ($E \cong 24.1$

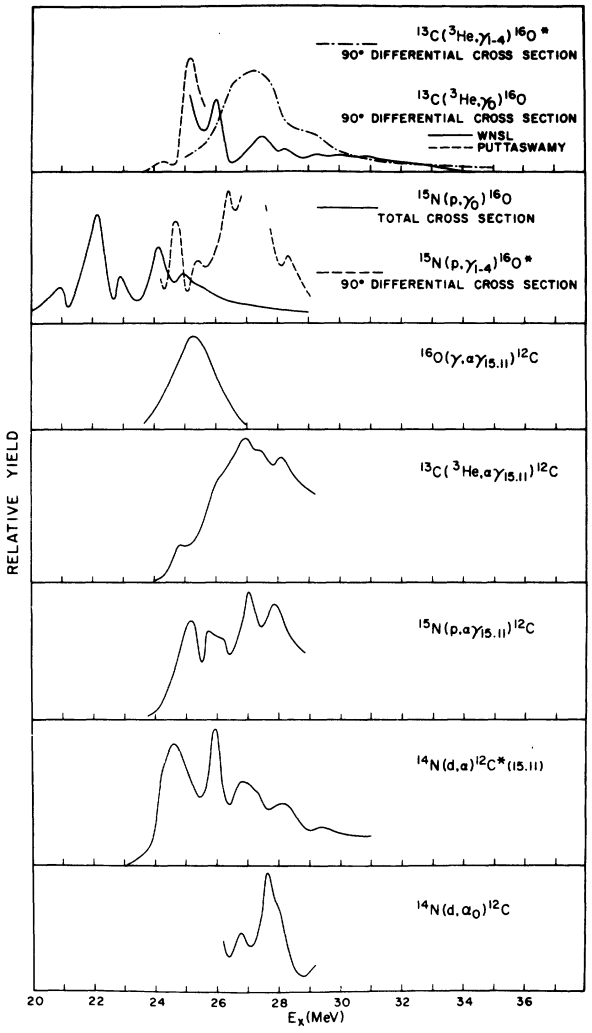


FIG. 29. Comparison of reaction exciting levels in $^{16}$O. All yields are relative. The ordinates for $^{13}C$-$(^3He,\gamma_{1-4})^{16}O$ and $^{15}N(p,\gamma_{1-4})^{16}O$ do not have the same scales as those of $^{13}C(^3He,\gamma_0)^{16}O$ and $^{15}N(p,\gamma_0)^{16}O$, respectively. The references for these yield curves are the following: $^{13}C(^3He,\gamma)^{16}O$, Puttaswamy (Ref. 23) and WNSL; $^{15}N(p,\gamma)^{16}O$, O'Connell (Ref. 11); $^{16}O(\gamma,\alpha\gamma_{15.11})$-$^{16}O$, Caldwell (Ref. 38); $^{13}C(^3He,\alpha\gamma_{15.11})^{16}O$, Weller, Van Rinsvelt, and Dunnam (Ref. 35); $^{15}N(p,\alpha\gamma_{15.11})^{12}C$, O'Connell (Ref. 11); $^{14}N(d,\alpha\gamma_{15.11})^{12}C$, Browne (Ref. 36); $^{14}N(d,\alpha_0)^{12}C$, Chaudir (Ref. 39).

MeV) is responsible for the resonances seen in $(^3He, \gamma_0)$, $(p, \gamma_0)$, and $(\gamma, n_0)$.

The appearance of resonances at 24.1 and 25.2 MeV in both helion and nucleon radiative capture indicates that these states may be comprised of a roughly equal admixture of 1p-1h and 3p-3h configurations. We may obtain a rough estimate of the helion reduced width for the 25.22-MeV state from a comparison of the $^{15}N(p, \gamma_0)^{16}O$ data and our $^{13}C(^3He, \gamma_0)^{16}O$ data. Using the Breit-Wigner relation for an isolated level, one obtains for the ratio of helion and proton widths $\Gamma_h/\Gamma_p = 0.075$ (0.047), where the first figure is based on Tanner's normalization, the second on O'Connell's. If only the ground-state proton, neutron, and helion partial widths contribute appreciably to the total width of the state $\Gamma \simeq \Gamma_p + \Gamma_n + \Gamma_h$, then the measured value of $\Gamma$, 0.46 MeV, implies, for $\Gamma_p \simeq \Gamma_h$, $\Gamma_{^3He} \simeq 0.017$ (0.011) MeV and $\Gamma_p = 0.221$ (0.224) MeV. Since angular distributions imply predominantly $s$-wave helion capture and $d$-wave proton capture, $|\gamma_p| \simeq 0.259$ $(MeV)^{1/2}$ and $|\gamma_h| \simeq 0.097$ (0.078) $(MeV)^{1/2}$. This helion reduced-width amplitude provides a benchmark for the detailed calculations to be presented below.

At higher excitations the proton-capture yields fall fairly monotonically; helion capture, on the other hand, exhibits pronounced structure between the excitation energies of 25 and 29 MeV. The $^{13}C(^3He, \gamma_{1-4})^{16}O$ reaction (Fig. 29) has very large cross sections in this region as does the reaction $^{15}N(p, \gamma_{1-4})^{16}O$, [11] which appears to have a very similar yield curve. Its shape, a broad maximum around 27.0 and 27.7 MeV, is shared with certain variations by a number of reactions, including $^{15}N(p, \alpha\gamma_{15.11})^{12}C$, (Ref. 11), $^{13}C(^3He, \alpha, \gamma_{15.11})^{12}C$, [35] and $^{14}N(d, \alpha\gamma_{15.11})^{12}C$. [36] One might expect that states in $^{16}O$ thus populated would have $T = 1$ since the 15.11-MeV state of $^{12}C$ has $J^\pi$, $T = 1^+$, 1 and has isospin purity better than 97%. [37] Of course, since the reaction $^{14}N(d, \alpha\gamma_{15.11})^{12}C$ is isospin forbidden, it proceeds via isospin impurities with only 3.1% of the strength of the allowed $^{14}N(d, \alpha\gamma_{12.71})^{12}C$, [36] but nevertheless its structure parallels that of the others. The common diminution of $\alpha$-particle yield to the 15.11-MeV state of $^{12}C$ below 25 MeV can be attributed to the Coulomb barrier for $s$-wave $\alpha$ particles at roughly 24.7 MeV, but the penetrability for $p$-wave $\alpha$ particles rises quickly enough so that resonating states need not definitely have a $J^\pi = 1^+$ assignment.

Other reactions with interesting structure in this region are $^{16}O(\gamma, \alpha\gamma_{15.11})^{12}C$ [38] and $^{14}N(d, \alpha_0)$-$^{12}C$, [39] the latter selecting only $T = 0$ states, with one in particular at 27.6 MeV. Weller, Roberson, and Tilley[40] assert that their $^{13}C(^3He, \alpha)^{12}C$ data imply that $T = 0$ states exist at 27.6 and 28.3 MeV and $T = 1$ levels at 26.9, 27.4, and 28.0 MeV, that the 27.6-MeV state has $J^\pi = 3^-$, [35] and that these states have large $\alpha$ widths. None of these other experiments yield significantly more detailed information on this region. The large variety of reactions resonating at the same energies that the $^{13}C(^3He, \gamma_0)^{16}O$ and $^{13}C(^3He, \gamma_{1-4})^{16}O$ reactions peak does tend to confirm, however, that these reactions proceed via compound nuclear resonances. The fact that the resonances in these reactions are clustered within 5 or 6 MeV of the helion escape threshold is an important clue. At higher energies, the number of available helion decay channels increases dramatically. States decaying primarily by the emission of a helion (or triton, for example) would have greater decay widths for the higher excitation energies. Thus, helion-capture cross sections would dwindle at higher energies because of the greater escape widths. States decaying primarily by proton or neutron emission would not exhibit such behavior since those escape thresholds are so much lower. This phenomenon is observed in the several decay channels of both $^9Be(^3He, \gamma)^{12}C$ and $^{13}C(^3He, \gamma)^{16}O$ and is, therefore, a strong indication of the structure of the states being populated; we may be observing a hallmark of "quasibound" states. A naive estimate of the excitation energy of a 3p-3h state would indicate $E \cong 3\hbar\omega \cong 45$ MeV. To appear as low as 25 to 30 MeV, a 3p-3h state must have strong correlations and thus would almost be bound to the emission of a single nucleon.

Parker and Cobern[41] have recently completed preliminary investigations of the triton transfer reaction $^{13}C(^7Li, \alpha)^{16}N$ and have found that this reaction populates $^{16}N$ states of excitation 11.1, 11.7, 12.4, 13.8, and 14.5 MeV which correspond to excitations of 24.1, 24.7, 25.4, 26.8, and 27.5 MeV in $^{16}O$. Several of these $T = 1$ levels may well be analogs of the states populated by the $^{13}C(^3He, \gamma_0)$-$^{16}O$ reaction.

Other radiative cluster capture experiments have been conducted corresponding to excitation energies below 25 MeV [$^{14}N(d, \gamma_0)^{16}O$ [42,43] and $^{12}C(\alpha, \gamma_0)$-$^{16}O$ [44]] with one resonance in the giant-resonance region observed in each reaction, at 22.71 and 21.05 MeV, respectively. On the basis of angular distributions, Suffert asserts that the state of 21.05 MeV may rather certainly be given the assignment $1^-$, 1, although this would necessitate $\alpha$-particle capture via isospin impurities. This hypothesis is not in the least improbable since Wu, Firk, and Phillips[12] quote the largest isospin mixing amplitude ($\leq 0.2$) in this range, $20 < E_x < 21$ MeV. The assignment of the other resonance is considerably more problematic. Suffert feels most confident in assigning it $1^+$, despite the fact

that the assignment would either break isospin in the entrance channel for $1^+, 1$ or be in serious contradiction to Morpurgo's inhibition for $M1$, $\Delta T = 0$ radiation. Moreover, a more recent experiment[43] finds the resonance energy higher by 130 keV and 22.84 MeV and thus corresponding rather exactly to the 22.84-MeV resonance seen in proton capture.[10] This new measurement casts serious doubt upon the conjecture of Gillett, Melkanoff, and Raynal[14] that this is a 2p-2h state and responsible for the interference dip in the $^{16}O(\gamma, n_0)^{15}O$ [12,45] and $^{15}N(p, \gamma_0)^{16}O$ [10,11] cross sections. With the more recent resonance energy the assignment $1^-, 1$ becomes more probable. Although this result contradicts Gillet's model explaining the structure of the $^{16}$O giant resonance in terms of destructive interference between states consisting mainly of 1p-1h or 2p-2h configurations, it does not directly strengthen the position of the 3p-3h model of Shaken and Wang.[15] Indeed, these experiments may be seen to imply that 4p-4h and 2p-2h configurations contribute significantly to the states resonating at roughly 21.0 and 22.8 MeV, respectively, in $(\gamma, p_0)$ and $(\gamma, n_0)$.

For a consistent choice of normalization, the ratio of average $\gamma_0$ yields for proton and helion capture into $^{16}$O is $R = 1/12.5$, a value closely matching the ratio of $^{12}$C, $r_1 = 1/11.8$ (the ratios $R$ and $r_1$ are defined in Table III). If the secondary doorway model discussed earlier were to apply to both of these reactions, then the equality of these ratios implies that the average helion reduced widths of the secondary doorways are equal.

A comparison of the average yields for $^{15}N(p, \gamma_{1-4})^{16}O$ and $^{13}C(^3He, \gamma_{1-4})^{16}O$ would be interesting, but unfortunately O'Connell[11] did not indicate the normalization of his $^{15}N(p, \gamma_{1-4})^{16}O$ data with respect to his $^{15}N(p, \gamma_0)^{16}O$ data. To obtain a crude estimate of this normalization, the $^{15}N(p, \gamma_0)^{16}O$ and $^{15}N(p, \gamma_{1-2})^{16}O$ data of Barnett and Tanner[10] have been compared with those of O'Connell at the overlap point, $E_x \simeq 24$ MeV (Table III). The averaged branching ratio of $\gamma_0$ and $\gamma_{1-4}$ decays is $\geq 1.25$ for proton capture while $\cong 10.0$ for helion capture. This glaring contrast highlights the point that the group of states 25–29 MeV have large deuteron, helion, and $\alpha$ widths. One would then expect that the first four excited states fed by decays $\gamma_{1-4}$ are comprised of fairly complex configurations. The investigations of the $0^+, 0$, 6.05-MeV and $2^+, 0$, 6.92-MeV levels by elastic $\alpha$ scattering[46] (to the higher $4^+$ and $6^+$ members) and $\alpha$-particle transfer[47] experiments indicate that these are the first two members of a 4p-4h rotational band; several theoretical treatments[48–50] have successfully reproduced this structure. While early 1p-1h treatments[1,3] were unsuccessful in predicting the energies of the $3^-, 0$, 6.13-MeV and the $1^-, 0$, 7.12-MeV states, more recent calculations[49,50] show that a mixture of 1p-1h and 3p-3h configurations can give the proper energy levels and greatly improve the theoretical $B(E2, 1^- \rightarrow 3^-)$, formerly too small by an order of magnitude. Brown's later calculations,[51] in particular, demonstrated that the $1^-$ states at 7.12 and 9.59 MeV have equal admixtures of 1p-1h and 3p-3h components. The very strong $^{13}C(^3He, \gamma_{1-4})^{16}O$ yield is thus wholly consistent with the $^{13}C(^3He, \alpha\gamma_{15.11})^{12}C$, $^{15}N(p, \alpha\gamma_{15.11})^{12}C$, and $^{14}N(d, \alpha\gamma_{15.11})^{12}C$ results which also exhibit strong peaking in this range $27 \leq E_x \leq 28$ MeV.

### 5. $R$-MATRIX CALCULATIONS

We present here the yield curves and angular distributions of the reactions $^{15}N(p, \gamma_0)^{16}O$ and $^{13}C(^3He, \gamma_0)^{16}O$ predicted by an $R$-matrix calculation based on the Wang-Shakin wave functions.[15] These wave functions, which assume a closed-core $^{16}$O ground state, have $J^\pi = 1^-$, $T = 1$ and are linear combinations of 1p-1h and 3p-3h configurations. The version of the wave functions used here differs by a small modification from that presented by Wang and Shakin; a slightly different energy has been assigned to the $1^-, 0$ 1p-1h basis boson. Wang and Shakin identified the $1^-, 0$ basis boson with the state 7.12 MeV. Following the suggestion of Brown and Green[48] we have assumed that neither the 7.12-MeV state nor the 9.59-MeV state is a pure 1p-1h state and that the $1^-, 0$ basis boson may

TABLE III. Average cross sections of radiative capture reactions in $^{16}$O and their ratios.

| Reaction | Energy range (MeV) | Average 90° differential cross section ($\mu$b/sr) $\gamma_0$ decay | $\gamma_{1-4}$ decays |
|---|---|---|---|
| $^{15}N(p,\gamma)^{16}O$ | 20–29 [a] | 3.45 | ... |
| | 24.5–29 [a] | 2.31 | $\geq 2.9$ [b] |
| $^{13}C(^3He,\gamma)^{16}O$ | 23.6–35 [c] | 0.105 | 0.95 |
| | 24.5–29 | 0.184 | 1.85 |

Ratios of cross sections averaged over the energy interval 24.5–29 MeV

$$R \equiv \frac{\sigma[^{13}C(^3He,\gamma_0)^{16}O]}{\sigma[^{15}N(p,\gamma_0)^{16}O]} = 1.12.5$$

$$R_{12} \equiv \frac{\sigma[^{15}N(p,\gamma_{1-4})^{16}O]}{\sigma[^{15}N(p,\gamma_0)^{16}O]} \geq 1.25$$

$$R_{22} \equiv \frac{\sigma[^{13}C(^3He,\gamma_{1-4})^{16}O]}{\sigma[^{13}C(^3He,\gamma_0)^{16}O]} = 10.0$$

[a] O'Connell (Ref. 11) normalized by factor of 1/1.6.
[b] O'Connell (Ref. 11) normalized by comparison with $^{15}N(p,\gamma_{1-2})^{16}O$ of Tanner and Barnett (Ref. 10).
[c] This work plus data of Puttaswany (Ref. 23) normalized to ours in region of overlap (1/1.6).

be assigned an energy between these two states. For simplicity, the space of $1^-, 1$ states has been truncated to include only those with the greatest $\gamma_0$ decay strength. These eight states are linear combinations of seven 3p-3h and two 1p-1h configurations. The 1p-1h configurations are in turn constructed from five $l_j(l'_{j'})^{-1}$ configurations $(J^\pi = 1, T = 1)$: $1s_{1/2}\,1p_{3/2}^{-1}$, $1d_{5/2}\,1p_{3/2}^{-1}$, $1d_{3/2}1p_{3/2}^{-1}$, $1d_{3/2}1p_{1/2}^{-1}$, and $2s_{1/2}1p_{1/2}$. These two 1p-1h configurations with unperturbed excitations 24.45 and 22.31 MeV carry most of the electric dipole strength expected for $^{16}$O and represent, therefore, the primary doorway state discussed earlier. By using Iachello's interacting boson model,[52] Wang and Shakin have demonstrated that the 3p-3h $1^-, 1$ configurations have excitation energy considerably lower than $3\hbar\omega$ and that they mix strongly with the 1p-1h primary doorways. They are, then, the secondary doorways which, to good approximation, account for the mixing of the 1p-1h primary doorways with the vast number of neighboring states.

The central assumptions of the present calculation are:

(1) Since the wave functions have only $J^\pi = 1^-$, $T = 1$ we may consider those $\gamma_0$ decays which are electric dipole transitions.

(2) Only 1p-1h configurations have nonzero $E1$ matrix elements for $\gamma$ decays to the closed-shell ground state. This limitation is imposed by the set of wave functions and severely restricts the usefulness of this calculation. One expects that transitions of the form 3p-3h → 2p-2h do play an important role in helion radiative capture, but Wang and Shakin have not included 2p-2h components in the ground-state wave function.

(3) The ground states of $^{15}$N and $^{15}$O may be approximated by the $(p_{1/2})^{-1}$ configuration and their third excited states by $(p_{3/2})^{-1}$. Thus, the Wang states are coupled to the neutron and proton ($s_{1/2}$, $d_{5/2}$, and $d_{3/2}$) decay channels only by the 1p-1h configurations.

(4) The ground state of $^{13}$C is considered to be $(p_{1/2})^{-3}$. Only the 3p-3h configurations are coupled to the two (the $s_{1/2}$ and $d_{3/2}$ channels feeding the $^{13}$C ground state) helion decay channels. These are actually two separate assumptions since, as Arima[53] has pointed out, even if $^{13}$C were to consist of pure $(p_{1/2})^{-3}$, other configurations might also contribute large helion widths.

(5) The states excited in $^{16}$O have significant decay widths only for the emission of neutrons, protons, and helions to the ground states of $^{15}$O, $^{15}$N, and $^{13}$C and of neutrons and protons to the third excited states of $^{15}$O and $^{15}$N, respectively. The branching ratios for $^{16}$O$(\gamma, n)^{15}$O and $^{16}$O$(\gamma, p)^{15}$N have been measured by Caldwell, Fultz, and Bramblett.[54] These indicate that decays to these one-hole states (ground and third excited states of $^{15}$O and $^{15}$N) account for some 78% of the total $\gamma$ absorption cross section. Branching ratios to the other excited states as well as to other decay channels (e.g., $\alpha$-particle emission to the 15.11-MeV $T = 1$ state in $^{12}$C) are comparatively small. Triton widths are here assumed, as a matter of expedience, to be smaller than helion widths.

(6) Helion channels may be treated by an $R$-matrix formalism in a manner completely analogous to the treatment of nucleon channels.

The principal parameters entering the calculations are these:

(1) $E_\lambda$, the resonance energy of state $\lambda$, is given by the Wang wave functions.

(2) $C_{\beta\lambda}$, the coefficient of the configuration $\beta$ appearing in the expansion of the state $\lambda$, is also given by Wang's wave functions.

(3) There are four open nucleon channels (neutron and proton, $s$ and $d$ wave) leading to the $\frac{1}{2}^-$ ground states of $^{15}$N and $^{15}$O and six open nucleon channels leading to the $\frac{3}{2}^-$ third excited states of these nuclei. The value of the wave function at the channel radius (5 fm for all channels), which is determined in optical-model calculation, is used to form a crude estimate of the reduced width amplitudes for these channels:

$$\gamma_{\beta' c} = \pm\frac{\hbar c}{2}\frac{1}{m_c c^2 R_c} F R_c u_{nl}(R_c), \quad \text{in (MeV)}^{1/2}, \tag{2}$$

where $\beta'$ and $c$ are the configuration and channel indices, $m_c$ is the channel reduced mass, $R_c$ is the channel radius, and $u_{nl}(R_c)$ the nucleon wave function evaluated at the channel radius. The term $F$ is the parentage factor representing the probability that the configuration $\beta'$ minus the $2s$ or $1d$ nucleon be the residual state of $^{15}$O or $^{15}$N. The factor $F$ is set equal to 1 for configurations with $p_{1/2}$ holes and for channels leading to the $^{15}$O and $^{15}$N ground states. For the configurations with $p_{3/2}$ holes and for channels leading to the $^{15}$O and $^{15}$N third excited states, the branching ratios of Caldwell, Fultz, and Bramblett[54] (within the context of Wang and Shakin's wave functions) imply that $|F| \cong 0.37$.

(4) The $E1$ reduced matrix elements of the 1p-1h configurations are estimated from these same optical-model wave functions.

(5) There are two open helion channels ($s$ and $d$ partial waves to the state of $^{13}$C). Their reduced width amplitudes for each 3p-3h configuration are taken as free parameters, but we assume the range of reasonable values to be delimited by product of the Wigner limit $[\frac{3}{2}(\hbar^2/m_c R^2)]^{1/2}$ and the isospin Clebsch-Gordan coefficient. This value

[0.716 (MeV)$^{1/2}$] contains no nuclear structure information and must be considered an extreme upper limit. The reduced width amplitude extracted directly from the data for the 25.22-MeV resonance is much smaller ($0.078 \leq |\gamma_{^3\mathrm{He}}| \leq 0.097$ MeV).

The $R$-matrix formalism used here, as well as the expressions for the $E1$ reduced matrix elements, are derived by Brassard[6] in a self-consistent treatment. Shay[20] gives the complete details of the calculation whose results are cited here.

The differential cross section is computed from the Blatt and Biedenharn relation:

$$\frac{d\sigma}{d\Omega}=\frac{1}{k_c^2(2I+1)(2S+1)}\sum_{\nu tt'} T_t^* W_{tt'}^{(\nu)} T_{t'} P_\nu(\cos\theta),$$

where $W_{tt'}$ is the vector coupling coefficient and $T_t$ is the transition amplitude for the transition $t$. The index $t$ denotes a reaction proceeding from a specific incoming channel and decaying via a specific $\gamma$ channel. Assuming that the electromagnetic widths of the excited states are small, $T_t$ is then proportional to the sum of the products of probability amplitudes for the population of states $\lambda$ (all of spin $J$) via the channel $lj$ and for the subsequent $\gamma$ decay $L\omega$, of these states to the ground state, $|X\rangle$:

$$T_t=\left(\frac{k_\gamma}{\hbar}\right)^{1/2}\sum_\lambda T^J_{\lambda;lj}\langle \lambda J\| T_L^{(\omega)}\| X\rangle .$$

We write the well-known expression for $T^J_{\lambda;lj}$ in matrix notation

$$T^J_{\lambda;lj}=\left(\frac{\hbar}{2}\right)^{1/2}\frac{\gamma_\lambda^T}{E_\lambda-E}[1-(R+d)^{-1}(R+d)^*]L,$$

where $\gamma_\lambda$ is the vector of reduced widths $\gamma_{\lambda c}$ for the state $\lambda$; $R$ is the familiar $R$ matrix

$$R_{cc'}=\sum_\lambda \frac{\gamma_{\lambda c}\gamma_{\lambda c'}}{E_\lambda-E};$$

and $d$ and $L$ are the diagonal matrices found from the vector of incoming wave solutions ($I$) ($d^*=IL^{-1}$ and $L=I-bI$). For charged-particle channels $I_{cc}$ is computed from Coulomb wave functions; for the neutron channel, from spherical Bessel functions. To assure that the resonance energies equal the state energies we have used the channel boundary condition $b_{cc}=-1$. The reduced widths and $E1$ matrix elements are calculated as outlined above.

The predicted yields and $A_2$ coefficients of the $^{15}$N$(p,\gamma_0)^{16}$O and $^{13}$C$(^3$He$,\gamma_0)^{16}$O reactions are shown by the solid lines in Fig. 30. The long-short dashed lines are the $^{15}$N$(p,\gamma_0)^{16}$O data of O'Connell[11] and the $^{13}$C$(^3$He$,\gamma_0)^{16}$O data of Puttaswamy,[23] with their normalization reduced by a factor of 1.6 for demonstration purposes. The solid circles are our $^{13}$C$(^3$He$,\gamma_0)^{16}$O data. The dashed lines represent the theoretical prediction averages over 300-keV intervals to simulate experimental resolution poorer than that of the several experiments. The value of $F=0.40$ was used in this calculation, and the absolute values of the reduced helion widths typically fall in a range $0.05 \leq |\gamma_h| \leq 0.40$, wholly consistent with the expected values. The predicted $^{15}$N$(p,\gamma_0)^{16}$O cross section reproduces the experimental data rather well, except for the resonance at 24.2 MeV. As mentioned above, the

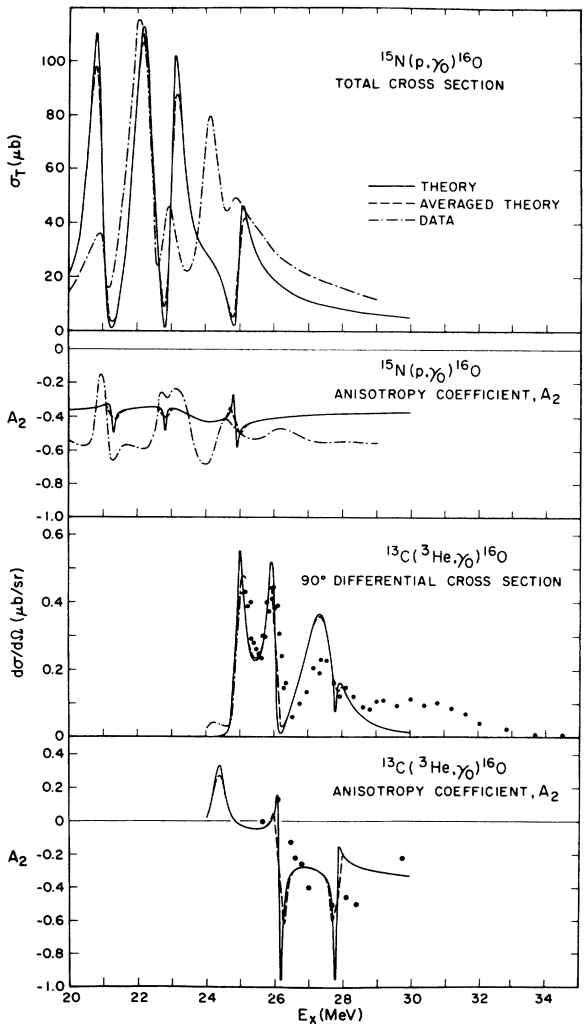


FIG. 30. Predicted $^{15}$N$(p,\gamma_0)^{16}$O and $^{13}$C$(^3$He$,\gamma_0)^{16}$O cross sections and $A_2$ anisotropy coefficients are shown as the solid and dashed (averaged over 300-keV interval) lines. Our data are depicted as darkened circles. O'Connell's $^{15}$N$(p,\gamma_0)^{16}$O data and Puttaswamy's $^{13}$C-$(^3$He$,\gamma_0)^{16}$O data are illustrated by the long-short dashed lines.

exact position of these resonances depend upon the eigenenergies assigned to the 1p-1h basis bosons. Since the over-all normalization of the $^{15}N(p,\gamma_0)$-$^{16}O$ $A_2$ coefficient is insensitive to any of the free $R$-matrix parameters its relative success in reproducing the measured $A_2$ coefficients constitutes, then, a major endorsement for the secondary doorway hypothesis: an explanation for the small variation in the shape of the angular distributions in a region of very strong intermediate structure. The total cross sections and $A_2$ coefficients appearing in the articles of Barrett *et al.*[55] and of Sarius and Marangoni[5] illustrate, by contrast, the results of 1p-1h calculations. The calculated $^{13}C(^3He,\gamma_0)^{16}O$ 90° excitation function and $A_2$ coefficients are highly sensitive to changes in helion reduced widths. Their reproduction of the data cannot, then, be viewed as particularly outstanding. One point is, however, emphasized by this aspect of the calculation. The model states at 26.0, 27.6, and 28.0 MeV are predominantly comprised of 3p-3h configurations, with very small 1p-1h admixtures (unlike the model states at 24.2 and 25.0 MeV, which are primarily 1p-1h and which produces resonances in both reactions). Even so, their small 1p-1h component suffices to mediate the $\gamma_0$ transition. As a consequence of their small 1p-1h components, little structure is predicted for $^{15}N(p,\gamma_0)$-$^{16}O$ in that energy range. The fact that little structure is seen above $E_x = 26.0$ MeV in the $^{15}N(p,\gamma_0)^{16}O$ experimental excitation function, thus does not necessarily imply that the structure observed in helion radiative capture cannot arise from transitions mediated by the same 1p-1h configurations responsible for most of the radiative proton-capture strength. This point may apply in $^{12}C$ also; we cannot conclude from the lack of structure in $^{11}B(p,\gamma_{0,1})^{12}C$ that the $\gamma$ transitions in helion capture are necessarily of the form 3p-3h → 2p-2h.

## 6. CONCLUSIONS

Strong resonance structure has been found in the regions immediately above the helion thresholds in $^{12}C$ and $^{16}O$. These may be interpreted as quasi-bound states which are predominantly 3p-3h in nature. Their $\gamma$ deexcitations transitions have been observed to be predominantly electric dipole radiation. Evidence for strong $E2/M1$ contributions is observed, however, in $^{16}O$.

These data and the detailed comparison with calculations based on 1p-1h, 3p-3h wave functions strongly suggest that 3p-3h configurations may play a significant role in the intermediate structure of the $^{12}C$ and $^{16}O$ giant resonance. The resonances and 24.2 and 25.1 MeV in $^{16}O$, in particular, may arise from states comprised of 1p-1h and 3p-3h configurations. Neither the data nor the calculation exclude, however, the possibility that the $\gamma_0$ decays are proceeding via transitions of the form 3p-3h → 2p-2h, an indication of ground-state correlations. The 28.84-MeV resonance seen in both $^9Be(^3He,\gamma_0)^{12}C$ and $^9Be(^3He,\gamma_2)^{12}C$ does indeed lend credence to this view. Since the relative strength of the decays to the excited states is much greater than in proton capture, these data may directly reveal giant resonances built on multiparticle multihole excited states.

The $R$-matrix calculation is premised on a very restrictive set of assumptions. The use of $1^-, 1$ wave functions excludes the possibility of accounting for the large $A_1$ coefficient observed above 26.0 MeV in $^{13}C(^3He,\gamma_0)^{16}O$. The representation of the ground state of $^{16}O$ as a closed core precludes the hope of evaluating the relative importance of 3p-3h → 2p-2h and 1p-1h → core transitions in the $\gamma_0$ decays. The calculation did, however, indicate the utility of the secondary doorway hypothesis for explaining intermediate structure. Its success in predicting the $^{15}N(p,\gamma_0)$-$^{16}O$ $A_2$ coefficient is especially notable. The general features of the $^{13}C(^3He,\gamma_0)^{16}O$ excitation function and angular distributions are well predicted by these calculations. A more sophisticated theoretical treatment, including ground-state correlation and $1^+$ and $2^+$ excitations, then, promises to be fruitful.

## ACKNOWLEDGMENTS

The authors would like to thank Dr. P. D. Parker, Dr. A. Gobbi, Dr. W. D. Metz, Dr. M. Fritts, Dr. M. Sachs, and Dr. F. W. K. Firk for their advice and help. Thanks are especially extended to D. Pisano who built and maintained the helium-3 recirculating system. We are pleased to acknowledge our gratitude to the staff of the Wright Nuclear Structure Laboratory.

†Work supported by U. S. Atomic Energy Commission Contract No. AT(11-1)-3074.

*Present address: Lawrence Livermore Radiation Laboratory, Livermore, California 94550.

[1] J. P. Elliott and B. F. Flowers, Proc. R. Soc. Lond. A242, 57 (1957).

[2] G. E. Brown and M. Bosterli, Phys. Rev. Lett. 10, 472 (1959).

[3]G. E. Brown, I. Castillego, and J. A. Evans, Nucl. Phys. 22, 1 (1961); N. Vinh-Mau and G. E. Brown, Nucl. Phys. 29, 89 (1962); V. Gillet and N. Vinh-Mau, Nucl. Phys. 54, 321 (1964).
[4]B. Buck and A. D. Hill, Nucl. Phys. A95, 271 (1967).
[5]A. M. Sarius and M. Marangoni, Nucl. Phys. A132, 433 (1969).
[6]C. Brassard, Ph. D. thesis, Yale University, 1970 (unpublished); C. Brassard, H. D. Shay, J. P. Coffin, W. Scholtz, and D. A. Bromley, Phys. Rev. C 3, 53 (1972).
[7]R. G. Allas, S. S. Hanna, L. Meyer-Schutzmeister, and R. E. Segel, Nucl. Phys. 58, 122 (1964).
[8]N. W. Reay, N. M. Hintz, and L. L. Lee, Jr., Nucl. Phys. 44, 338 (1963).
[9]G. Kernel and W. N. Mason, Nucl. Phys. A123, 205 (1969).
[10]N. W. Tanner, G. C. Thomas, and E. D. Earle, Nucl. Phys. 52, 29,451 (1964); A. R. Barnett and N. W. Tanner, Nucl. Phys. A152, 257 (1970); E. D. Earle and N. W. Tanner, Nucl. Phys. A95, 241 (1967).
[11]W. J. O'Connell, Ph. D. thesis, Stanford University, 1969 (unpublished).
[12]C.-P. Wu, F. W. K. Firk, and T. W. Phillips, Phys. Rev. Lett. 20, 1182 (1968); C.-P. Wu, Ph. D. thesis, Yale University, 1968 (unpublished).
[13]J. E. E. Baglin and M. N. Thompson, Nucl. Phys. A138, 73 (1969).
[14]V. Gillet and A. Melkanoff, and J. Raynal, Nucl. Phys. A97, 631 (1967).
[15]W. L. Wang, Ph. D. thesis, Massachusetts Institute of Technology, 1971 (unpublished); C. M. Shakin and W. L. Wang, Phys. Rev. Lett. 26, 902 (1971); C. M. Shakin and W. L. Wang, Phys. Rev. C 5, 1898 (1972).
[16]E. M. Diener, J. F. Amann, S. L. Blatt, and P. Paul, Nucl. Instrum. Methods 83, 109 (1970).
[17]M. Suffert, Nucl. Phys. 75, 226 (1966).
[18]W. Del Bianco and F. Lemaire, Nucl. Instrum. Methods 61, 229 (1968).
[19]P. D. Barnes, D. Biegelson, J. R. Comfort, and R. O. Stephen, Wright Nuclear Structure Laboratory Internal Report No. 25 (unpublished).
[20]H. D. Shay, Ph. D. thesis, Yale University, 1972 (unpublished).
[21]C. Brassard, Nucl. Instrum. Methods 94, 301 (1971).
[22]R. L. Bramblett, S. C. Fultz, B. L. Berman, M. A. Kelly, J. T. Caldwell, and D. C. Sutton, UCRL Report No. 70582, 1967 (to be published).
[23]N. G. Puttaswamy, Ph. D. thesis, Stanford University, 1966 (unpublished); N. G. Puttaswamy and D. Kohler, Phys. Lett. 20, 288 (1966).
[24]E. Ventura, E. M. Diener, C. E. Chang, and S. S. Hanna, report; Bull. Am. Phys. Soc. 17, 113 (1972).
[25]F. W. K. Firk, Annu. Rev. Nucl. Sci. 20, 39 (1970).
[26]R. W. Carr and J. E. E. Baglin, Nucl. Data A 10, 143 (1971).
[27]S. L. Blatt, K. J. Moon, and K. Kohler, Phys. Rev. C 6, 1536 (1972); K. J. Moon, Ph. D. thesis, Ohio State University, 1969 (unpublished).
[28]I. Linck and M. L. Kraus, C. R. Acad. Sci. (Paris) 275B, 669 (1972).
[29]V. Gillet, Ph. D. thesis, Universitê de Paris, 1963 (unpublished), p. 150.
[30]S. Cohen and D. Kurath, Nucl. Phys. 73, 1 (1965).
[31]D. Aggassi, V. Gillet, and H. Lumbruso, Saclay report (to be published).
[32]E. Obst, F. Rauch, and H. G. Wahsweiler, Nucl. Phys. A103, 17 (1967).
[33]Y. A. Glukhov, G. B. Novatskii, H. H. Ogloblin, S. B. Sakuta, and D. N. Stetzanov, Kurchatov Institute of Atomic Energy Report, 1969 (to be published).
[34]F. Ajzenberg-Selove, Nucl. Phys. A114, 1 (1968).
[35]H. R. Weller, H. A. Van Rinsvelt, and F. E. Dunnam, Phys. Lett. 27B, 283 (1968).
[36]C. P. Browne, Nucl. Phys. 66, 49 (1965).
[37]F. D. Reisman, P. I. Cannon, and J. B. Marion, Nucl. Phys. A153, 244 (1970).
[38]J. T. Caldwell, UCRL Report No. UCRL 50287 (unpublished).
[39]M. A. Chaudri, Ph. D. thesis, University of Heidelberg, 1964 (unpublished).
[40]H. R. Weller, N. R. Roberson, and D. R. Tilley, Phys. Lett. 25B, 541 (1967).
[41]P. D. Parker and M. Cobern, private communication.
[42]M. Suffert, Ann. Phys. (N.Y.) 1, 547 (1966).
[43]H. R. Weller, R. A. Blue, and S. L. Blatt, Phys. Rev. C 5, 648 (1972).
[44]M. Suffert and W. Feldman, Phys. Lett. 24B, 579 (1967).
[45]J. T. Caldwell, R. L. Bramblett, and B. C. Berman, Phys. Rev. Lett. 15, 976 (1967).
[46]E. B. Carter, G. E. Mitchell, and R. H. Davis, Phys. Rev. 133, B1421 (1964).
[47]F Puhlhofer, H. G. Ritter, R. Buck, G. Bremmundt, H. Schmidt, and K. Bethge, Nucl. Phys. A147, 258 (1970); P. D. Parker and M. Cobern, private communication.
[48]G. E. Brown and A. M. Green, Nucl. Phys. 75, 401 (1966).
[49]L. S. Celenza, R. M. Dreizler, A. Klein, and G. J. Dreiss, Phys. Lett. 23, 241 (1966).
[50]A. P. Zucker, B. Buck, and J. B. McGory, Phys. Rev. Lett. 21, 39 (1968).
[51]G. E. Brown, Phys. Lett. 15, 168 (1965).
[52]F. Iachello, Ph. D. thesis, Massachusetts Institute of Technology, 1969 (unpublished).
[53]A. Arima, private communication.
[54]J. T. Caldwell, S. C. Fultz, and R. L. Bramblett, Phys. Rev. Lett. 19, 447 (1967).
[55]R. F. Barrett, L. C. Briedenharn, M. Danos, P. P. Delsanto, W. Greiner, and H. G. Wahsweiler, Rev. Mod. Phys. 45, 44 (1975).